UNLIMITED

RSRE
MEMORANDUM No. 4305

ROYAL SIGNALS & RADAR ESTABLISHMENT

SIMPLE GRAPHICAL DESCRIPTIONS OF NATURAL LAND PROFILES AND THE APPLICATION OF FRACTAL AND SUB-FRACTAL MODELS TO THEM

Author: D L Jordan

PROCUREMENT EXECUTIVE,
MINISTRY OF DEFENCE,
R S R E MALVERN,
WORCS.

RSRE MEMORANDUM No. 4305

CONDITIONS OF RELEASE

0059819 BR-112563

********** U

********** Y

Reports quoted are not necessarily available to members of the public or to commercial organisations.

****

DCAF CODE 090996

ROYAL SIGNALS AND RADAR ESTABLISHMENT

Memorandum

4305

TITLE: SIMPLE GRAPHICAL DESCRIPTIONS OF NATURAL LAND PROFILES AND THE APPLICATION OF FRACTAL AND SUB-FRACTAL MODELS TO THEM

AUTHOR: D L Jordan

DATE: July 1989

SUMMARY

Terrain profiles from four widely different areas of Britain are obtained from Ordnance Survey maps and shown to be well modelled as either fractal or as a hierarchy of different fractals. The profiles are then smoothed using a crude small-scale smoothing method to allow them to be modelled as sub-fractal surfaces. Rays are drawn from these surfaces to simulate the scattering of incoherent radiation. The resulting ray density statistics are analysed and shown to be approximately Gamma-distributed. Based on the findings suggestions are made regarding possible methods of remotely determining surface texture for metrology purposes. The overall aim of this Memorandum is not mathematical rigour, but rather the use of simple pictorial methods as an aid to gaining a physical insight into rough surface scattering and how such information might be used in describing and measuring surface texture.

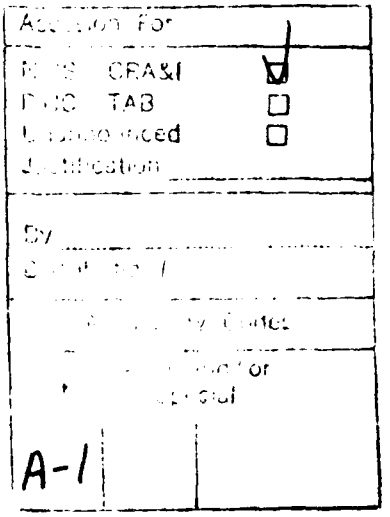

RSRE MEMORANDUM NO 4305

SIMPLE GRAPHICAL DESCRIPTIONS OF NATURAL LAND PROFILES AND THE APPLICATION OF FRACTAL AND SUB-FRACTAL MODELS TO THEM

D L Jordan

LIST OF CONTENTS

1 INTRODUCTION

Advances in remote sensing of solid surfaces for metrologic purposes have been made by modelling the surface as multi-scale or fractal in nature[1,2]. Unfortunately, it has so far proved impossible to define one or two simple and easily measured parameters that describe the surface texture. Similar (fractal) models may also have some application in describing natural land surfaces. In this memorandum an attempt, albeit somewhat crude, is made to judge whether a fractal model is appropriate in describing natural topographic surfaces. In section 2 it is shown that indeed the natural landscape in the four dissimilar regions of Britain studied does behave as fractal, or at least as a hierarchical arrangement of fractals having a relatively small range of dimensions.

The effect of introducing high frequency smoothing on to the terrain profiles converts them into a sub-fractal surface[3] and consequently allows rays to be drawn from them to simulate the scattering of radiation. The resultant ray density statistics are then investigated in sections 4 and 5 and shown to be consistent with a Gamma distribution. It is encouraging that this is in agreement with the large body of work on Synthetic Aperture Radar modelling[4,5,6,7] which has successfully modelled the terrain as a random distribution of scatterers with a gamma-distributed variation of cross-section from resolution cell to resolution cell. The effect of enhancing the non-gaussian nature of the scattering statistics by reducing the size of the illuminated region is described in section 6. The viability of using this approach to describe surface texture in metrology applications is also briefly discussed.

Although the work described in this memorandum is highly simplistic in its approach and somewhat lacking in precision it does nevertheless suggest that topographic features may be realistically modelled in terms of fractals, and that this has implications for digital mapping techniques. It also suggests a somewhat different approach to investigating surface texture for metrology purposes, a key topic in the commercial exploitation of any technique for remotely determining surface structure.

2 LAND PROFILES

Profiles were obtained from four separate areas of Britain; mid-Wales, Dartmoor, Huntingdonshire and Malvern. These cover both rugged and relatively flat areas and represent extremes of typical topographic areas. Profiles running north-south and east-west for each region were obtained from Ordnance Survey maps by reading off the contour heights and joining the points by a smooth curve. Although limited in resolution it probably allows a reasonable representation of the land profile at the larger scale sizes, say a few tens of metres upwards. The contours were given on the maps at 5 m intervals for the smooth regions and 10 m intervals for the hilly areas of Wales and Dartmoor. One profile from each area is shown in Figure 1; it should be noted that the highly compressed horizontal scale used in this memorandum leads to visually unrealistic land profiles. Figure 1a shows an east-west profile running from Hook Bank towards Elmley Castle (OS 800410-940410); a similar profile running north from Hook Bank towards Madresfield (OS 810411-810500) was also drawn. Although the changes in ground height are relatively small, some of them occur quite abruptly. The profile shown in Figure 1b corresponds to a north-south profile in Huntingdonshire (OS 280700-280800). Although similar to the previous profile in that the height variation is small, the terrain is more rounded. Another profile of this area running east-west was also obtained (200750-400750). Figure 1c shows a profile across Dartmoor (SX 470830-870830). This is totally different in character to the previous two shown; it is basically two sides of a triangle with a considerable amount of deep but relatively narrow flat-topped structure superimposed on it. Finally the last profile shown (Figure 1d) is of an area around Painscastle in mid-Wales; the actual profile shown is an east-west transect (SO 000450-200450). A north-south profile (SO 090400-090500) was also drawn. Like the last profile this is also highly undulating, but unlike the Dartmoor sample is less obviously composed of a single large scale structure with smaller scales superimposed on it.

For each of the profiles the structure function $S(\delta)$ was calculated, the structure function being defined as

$$S(\delta) = \langle (h(x) - h(x+\delta))^2 \rangle \qquad (1)$$

where h(x) is the local surface height at position x. For a simple corrugated fractal[1]

$$S(\delta) = L^{2-\upsilon} |\delta|^{\upsilon} \quad \text{with} \quad 0 < \upsilon < 2 \qquad (2)$$

where the topothesey L is a measure of the average rate of change of height[8] and υ is related to a fractal dimension D by[9] $\upsilon = 2(2-D)$.

Both the power index υ and the topothesey can be determined from a plot of log S versus log δ; such plots for the various profiles shown in Figure 1 are shown in Figure 2. All the profiles display one or more straight line sections over limited ranges of scale sizes, indicating fractal behaviour. The fractal behaviour may well extend down to much smaller scales but the limited resolution/accuracy obtainable from Ordnance Survey maps precludes this area from investigation. As with all real surfaces an outer scale, or low-frequency cut-off exists beyond which fractal behaviour is not observed. Some of the plots show more than one region of fractal behaviour. In most cases the profiles appear to behave as fractals from scale sizes of some tens of metres up to scales of order 0.5 to 1 km; beyond this some then possess a different power and topothesey up to scales of several kilometres. This behaviour is entirely consistent with that found by Mark and Aronson[10] for seventeen areas in the USA. In their work the data was obtained from digital maps; the data used a regular square grid data structure with a horizontal spacing of 30 m and elevations recorded as integers in metres. Of the seventeen areas studied one had a structure function with a constant υ and L from smallest to largest scale studied, one had a dimension that appeared to vary continuously with scale, suggesting that a smoothly varying single-scale model[11] was more appropriate than a fractal one, and the remaining fifteen of them were well described by ranges of scales having a constant fractal dimension separated by distinct breaks. The breaks represented characteristic horizontal scales at which the surface behaviour changed substantially. They also found, in agreement with the results shown in Figure 2, that over short scales (below 0.5-1 km)

many of their geomorphic surfaces possessed high values of υ ($\sim$ 1.7). However for scales between this limit and several kilometres many areas were characterised by much lower values of υ (around 1–1.2). At even longer scales they found that the fractal model breaks down and can be replaced by periodicities. From Figure 2 is it apparent that the actual values of υ and L obtained for a given area are relatively insensitive to the actual positions and orientations within the area at which the profiles are determined; the east–west and north–south profiles of each area 'clump' together.

The results obtained in this work, like that reported by Mark and Aronson[10] has implications not only for geomorphology and for designing sampling schemes for digital maps, but also for terrain simulation for microwave imaging. Also the fact that different rractal dimensions are appropriate for different ranges of horizontal scales provides a possibly useful way of identifying characteristic landscape scales. Mark and Aronson[10] speculate that the scales at which the dimension changes represent scales at which the relative importance of different processes, of structural effects, and of time scales also change.

These findings also have implications for terrain sampling[10]. For areas having low values of υ the surface height autocorrelation is also low and so points cannot be accurately predicted from the heights of neighbouring points. Consequently a lot of information will be lost as the sampling interval is increased. Conversely when υ is high the surface is relatively smooth and hence the loss of precision with increasing sample interval is much less.

An indication of the relative importance of different surface features in producing the overall structure function versus scale plot can be obtained by considering a number of idealised profiles. A top hat or succession of top hat structures produces values of $\upsilon \sim 1$ and large values of L, whereas a series of delta functions (delta–correlated noise) gives rise to profiles with $\upsilon = 0$. A pure sinusoid and a straight sloping line lead to $\upsilon \sim 2$, $L \rightarrow 0$ because of their single scale, smoothly varying nature. A sum of differing frequency sinusoids however lowers υ and raises L; it also leads to a break in the

log $S(\delta)$ versus logδ plot. An example of this is shown in Figure 3. The actual profile shown in Figure 3a is a sum of sinusoids (plus a constant term); any one of them by itself gives rise to a linear structure function plot with $\upsilon \sim 2$ and no breaks in it until the outer scale is reached. When however several of these different frequency waves are added together to give the profile shown in Figure 3a, the resulting structure function plot has the form shown in Figure 3b. The region with $\upsilon = 1.7$ at low values of δ is due to the small period waves whereas the region at large δ with $\upsilon \simeq 2$ is due to the long period, large amplitude envelope. It is not clear what the shape of the intermediate region should be. Possibly if it is flat and has a positive slope it may mean that it is due to a dominant large period modulating smaller periods whereas if there is no one large dominant period, then a uniform gradient does not occur.

Further illustrations of the importance of various scale sizes and structure components in producing the overall structure function can be demonstrated by considering the Dartmoor profile shown in Figure 1c. If a smooth curve is drawn through the profile to produce the smoothed version shown in Figure 4a the structure function is changed to that shown in Figure 5. That is, it is changed to a smooth monotonically increasing straight line of slope $(= \upsilon) \simeq 2$, as expected for a smoothly varying profile. If now the largest of the smaller structures that 'ride on the back' of the smoothed profile are replaced, to produce the profile shown in Figure 4b, the resultant structure function (Figure 5) closely resembles the original one derived from the true profile.

Although pictorial in nature and lacking in rigour, this elementary discussion gives some insight into why the structure function plots possess the form shown in Figure 2. From both this work, and that discussed in reference 10 it seems reasonable to conclude that natural landscapes tend to produce values of υ in the range of just above unity to a maximum of around 1.8 for scale sizes less than 0.5–1 km, and often lower values of υ for larger scales. Man-made structures such as buildings and vehicles are generally more angular in nature than natural terrain features and consequently may be expected to produce values of $\upsilon \sim 1$ or even $\upsilon < 1$ if the features are anti-correlated. As single

man-made structures are generally quite small they only affect the small scale end of the structure function. However, a feature such as a town which covers a large range of scale sizes may well give rise to structure functions having lower values of v than are generally found for open countryside up to quite large scale sizes. For completeness the normalised profile height autocorrelation function $\rho(\delta)$, defined as

$$\rho(\delta) = \langle h(x)\ h(x+\delta)\rangle / \langle h^2 \rangle \qquad (3)$$

corresponding to the structure functions given in Figure 2 are shown in Figure 6; for clarity only one is shown for each area. The greater separation seen between the data from region to region when plotted in the linear format of the autocorrelation plots (Figure 6) rather than the logarithmic format of the structure function (Figure 2) suggests that there might be some advantages in dealing with autocorrelation functions rather than structure functions when looking for small differences in detailed structure.

As all the four areas of Britain studied seem to possess land profiles that can be realistically modelled as either fractal or a hierarchical arrangement of fractals with only a limited range of v-values it is of interest to consider how these areas may be remotely distinguished using some form of electromagnetic radiation. That is, some means of determining the surface texture is required. This is also a pressing problem in surface metrology and at present no satisfactory method exists of defining and measuring surface texture.

3 ANGULAR DISTRIBUTION OF SCATTERED COHERENT RADIATION

The angular distributions of coherent radiation scattered from a fractal surface whose roughness is large compared to the radiation wavelength is a sensitive function of v and L[1,11]. For a perfectly conducting surface the field in the Fraunhofer region is given in the tangent plane approximation by[12]

$$E = E_0 k F(\theta) \int_{-\infty}^{\infty} A(\underline{r}') \exp\{-i\underline{k}\cdot\underline{r}' G(\theta)\} \exp\{ikh(\underline{r}')f(\theta)\} d^2\underline{r}' \quad (4)$$

where E_0 is the incident plane wave field, k is the wavevector of the incident radiation ($= 2\pi/\lambda$), $A(\underline{r}')$ defines the variation of intensity within the illuminated region and $h(\underline{r}')$ is the local surface height at position $\underline{r}'$. F, G and f are angle dependent terms which for normal illumination are given by

$$\begin{aligned} F(\theta) &= 1 \\ G(\theta) &= \sin\theta \\ f(\theta) &= 1+\cos\theta \end{aligned} \quad (5)$$

where θ is the angle between the incident wave and the scattered one. From (4) the mean scattered intensity as a function of angle (θ) can be obtained in the Fraunhofer limit by using the fractal model given in (2) for the structure function and assuming joint-Gaussian height fluctuations as

$$\langle I(\theta)\rangle \propto k^2 \int_{-\infty}^{\infty} r dr\, J_0(kr\sin\theta) \exp\left\{-\frac{1}{2} k^2 L^{2-\upsilon} |r|^{\upsilon} (1-\cos\theta)^2\right\} \quad (6)$$

It is unfortunately necessary to perform the integration numerically for arbitrary values of υ. However, for the special case of an isotropic scatterer (the two dimensional analogue of the one dimensional Brownian scatterer) (υ=1) the integral may be evaluated analytically to give

$$\langle I(\theta)\rangle \propto \frac{(1+\cos\theta)^2}{\left\{\frac{1}{4} k^2 L^2 (1+\cos)^4 + \sin^2\theta\right\}^{3/2}} \quad (7)$$

The resulting calculated angular variation of the normalised mean intensity ($<I(\theta)>/<I(\theta=0)>$) is shown in Figure 7 for the case λ = 25 m. The values υ = 1.7, L = 10^{-4} m and 10^{-7} m have been taken as representative of the structure functions given in Figure 2 at small scale sizes and υ = 1, L = 0.1 m and 1.0 m at large scale sizes. From Figure 9 it can be seen that the angular distribution of mean scattered intensity changes quite dramatically with changes in either υ or L. Unfortunately it does not appear feasible to unambiguously determine both υ and L from a measurement of the angular distribution of mean scattered intensity[11].

4 SUB FRACTAL MODEL

Another possible method of remotely distinguishing between different areas ie distinguishing between the different surface textures may be to probe them with incoherent radiation. The data analysed so far indicates that the terrain profiles can be realistically modelled as either fractal or a hierarchical arrangement of fractals. Fractal surfaces are continuous but non-differentiable and hence mathematically the concept of rays is inappropriate. Consequently geometrical effects cannot occur; only diffraction and interference phenomena are generated. If however high frequency smoothing is applied to a fractal surface geometrical optics effects do occur and the concept of rays is entirely appropriate. Such a surface, which is both multi-scale and capable of generating geometrical optics effects is described by a sub-fractal model[3]. In this model the surface height is continuous and differentiable but its slope is fractal. Consequently the concept of rays is valid, but in the absence of higher surface derivatives, such as would occur for a continuous smoothly varying surface[13,14], no geometrical catastrophies occur in the scattered field. It may actually be that the distinction between fractal and sub-fractal surface models is a somewhat artificial mathematical division. If we consider for simplicity a one-dimensional profile that can be described as a Brownian fractal, then it arises from the limit of a random walk as the size of each contributing element tends to zero. As the elements are uncorrelated, then just prior to the size of each one tending to zero rays can be drawn from them; as the elements are randomly orientated a

uniform distribution of rays ensues. However, once the element sizes have been allowed to tend to zero, the surface is suddenly fractal and therefore continuous and non-differentiable and mathematically speaking, rays cannot in principle be drawn. Consequently it may in practical terms be better to think of a fractal surface not as continuous and non-differentiable, but as producing a uniform distribution of rays. The 'transition region' from sub-fractal to fractal presumably occurs when the element size becomes comparable to the wavelength λ. When the element size is greater than λ geometrical effects dominate and rays can be drawn from them giving a uniform distribution. However, when the element size becomes comparable with the wavelength diffraction phenomena dominate. The situation is of course much more complex in the two-dimensional case.

The necessary high frequency or small scale smoothing of the terrain profiles needed to justify the use of a sub-fractal model may actually be achieved naturally in practice. The smallest scale size that can realistically be obtained from ordnance survey maps is of order 10 m, and there is no way of knowing whether the terrain is still fractal below this limit, or whether there is an effective small scale smoothing occurring below some limiting scale size. Even if there is no such natural mechanism, the finite probing wavelength itself will constitute an effective inner scale smoothing, as will the use of wide bandwidth (incoherent) radiation. Whatever the justification, the profiles shown in Figure 1 were smoothed over small regions (typically 20-40 m) by an approximate 'top hat' integration

$$H(x) = \frac{1}{X} \int_{x-X/2}^{x+X/2} h(x')\, dx' \qquad (8)$$

where h is the local surface height derived from the original fractal profile. Although h is not differentiable H is once differentiable.

The most significant feature of scattering by a random surface governed by a fractal slope model is the dominant role played by the geometrical optics contribution to the scattered intensity pattern. Consideration of the resultant ray-density fluctuations also characterise fluctuations in intensity far from the scatterer in incoherent configurations. For coherent scattering, which will not be considered further in this memorandum, diffraction and interference as well as ray density fluctuations play a role.

5 RAY DENSITY FLUCTUATIONS

In all the work described here the problem is treated as one dimensional and the radiation is assumed to strike the surface in the form of a plane wave parallel to the horizontal axis. The statistical and correlation properties of the ray-density functional[3,15]

$$R = \frac{1}{z} \int \delta \left[m(x) - \frac{x}{z} \right] dx \qquad (9)$$

are investigated. This defines the ray density at a distant point z beyond the profile in the z = 0 plane which is corrugated in the x-direction and has a local random slope m(x). The terrain profiles were drawn by hand on paper at a scale of 1 cm ≡ 250 m. Rays were constructed normal to the surface at a rate of 8 rays cm^{-1} and the number of rays R entering a detector of fixed size (usually 1 cm) a given distance z above the mean profile height determined as the detector was scanned along. Although limited in accuracy this method should at least give an indication of the behaviour to be expected from probing the surface with incoherent radiation.

For all the profiles studied (one from each of the four areas) the normalised ray density moments $\langle R^n \rangle / \langle R \rangle^n$ were found to be a reasonable fit to a Gamma distribution

$$\frac{\langle R^n \rangle}{\langle R \rangle^n} = \frac{\Gamma(m+n)}{\Gamma(m)} \frac{1}{m^n} \qquad (10)$$

$$p(R) = \left[\frac{m}{\langle R\rangle}\right]^{m} R^{m-1} \frac{\exp\left[-\frac{mR}{\langle R\rangle}\right]}{\Gamma(m)} \qquad (11)$$

For the second normalised moment

$$\frac{\langle R^2\rangle}{\langle R\rangle^2} = 1 + \frac{1}{m} \qquad (12)$$

It should be emphasised that R is the number of rays per detector size. For each profile $\langle R\rangle$ and $\langle R^2\rangle$ were used to determine m; higher moments were then calculated from (10) and compared with the experimentally determined ones. The ray density probability distribution p(R) was also calculated and compared with an experimentally determined histogram; because of the limited sample size the histogram fluctuations were quite large.

Figure 8 shows the results from the Hook-Bank (E-W) profile. A detector size of 1 cm, corresponding to a real size of 250 m was used. The results shown correspond to a detector height of 120 m ie 10 cm above the mean profile height. Similar results were obtained for a reduced height of 70 m and an increased height of 170 m. As can be seen from Figure 8a the moments fit is quite good although the ray density appears to fluctuate slightly less than that predicted from (10) when using the value of m (= 2.9) calculated from (12); a better fit is obtained with m = 3.2. Figure 8c shows the normalised ray density autocorrelation function for three different heights. Although limited in resolution/accuracy it suggests that the correlation length is greater at heights of 120 m and 170 m than at 70 m, but there is no significant difference between the results for the two larger distances. The corresponding results for Huntingdon (E-W) are shown in Figure 9. In this case there is excellent agreement between the measured moments and those calculated using the experimentally derived values of m. Again there is some evidence for the ray density autocorrelation length being shorter for the smallest profile-detector height (70 m) than for greater heights.

Figure 10 shows the Painscastle (E-W) data. Unlike the previous two case where the detector size was 1 cm, it was only 0.5 cm in this case. Again, the ray density fluctuates less than that predicted on the basis of a Gamma distribution with m calculated from (12). The detector height was 640 m - 11 cm above the highest point on the profile. When the detector height was reduced to only 2-3 cm above the top of the profile the experimentally determined value of m was only reduced slightly (from 1.8 to 1.6). Again the ray density autocorrelation function falls off slightly faster closer to the surface than further away. Figure 11a shows the measured ray density contrast, defined as the standard deviation of the number of rays entering the detector to the mean number entering, as a function of detector size for the Painscastle profile. It indicates that, as expected, some detector aperture averaging is occurring with a 1 cm detector. Unfortunately with the relatively low density of rays it is practicable to draw, the inherent limitations of the method mitigate against using a much smaller detector. Figure 11b shows the contrast as a function of height above the surface for a fixed detector size of 2 cm; to derive this data the detector was moved along contours drawn parallel to the profile at different heights. The results for the Dartmoor profile are shown in Figure 12. Again a 1 cm detector was used and the results taken at a height of 740 m. Figure 12c shows the ray density autocorrelation function for two different detector sizes (5 mm and 10 mm).

Because of the relatively short profile lengths obtained from the Ordnance Survey maps it was not practicable to investigate large profile to detector distances (z). Consequently for the intermediate values of z investigated here the results cannot unambiguously be assigned to either the conventional Fresnel or Fraunhofer regimes. Consequently it is not possible to compare the measured ray density autocorrelation functions with theoretical predictions. For the Fresnel region the autocorrelation length is predicted[3,16] to increase nonlinearly with distance; for the case $\upsilon = 1$ it increases as z^2. The far-field condition is

$$\frac{1}{\ell}\left[\frac{z}{L_T^{\upsilon/2}}\right]^{\frac{z}{2-\upsilon}} \gg 1$$

where ℓ is the illuminated length, L is the topothesey and z is the profile to detector distance. Unfortunately equivalent theoretical derivations have not been published for the Fraunhofer region. All that can be tentatively concluded from these limited results is that the autocorrelation length does increase with z (in the range 20–170 m) but at a rate not greater than linearly, and may possibly saturate towards the higher values of z.

From the results presented in this memorandum which cover widely differing land profiles it seems reasonable to conclude that a small amount of profile smoothing results in a profile which is to some degree an approximation to a sub-fractal surface. In addition, the rays drawn from this profile have an approximate Gamma distribution. Interestingly this is the favoured model for synthetic aperture radar (SAR) modelling where it is found[4] that the resultant measured intensity, which is K-distributed, can be considered as a convolution between an underlying Gamma fluctuation from the terrain and a Gaussian speckle pattern arising from the coherent illumination used.

Jakeman[3,15,17,18] has derived a large number of analytical results for the statistical properties of the ray density from a sub-fractal random phase screen. He has shown[15] that the ray density is indeed expected to be close to being Gamma ditributed for a wide range of values of υ (exactly Gamma distributed for υ = 1). He has also shown that the effect of an outer scale cut-off (finite correlation length) is that the ray density comprises a number of independent contributions, each of which will be approximately (or exactly if υ = 1) Gamma distributed with parameter m. The sum of N such contributions will also be Gamma distributed but with an increased index Nm. This leads to a reduced degree of fluctuation and may possibly be part of the reason that the normalised moments calculated using the measured value of m fluctuate more than the measured ones. Detector averaging will also reduce the measured fluctuations[4].

The ray density contrast $c = \{<R^2>/<R>^2 - 1\}^{\frac{1}{2}}$ is obviously related to m by $c^2 = 1/m$. A plot of this using the experimentally measured values of c and m is shown in Figure 13 to illustrate the range of values obtained from the different profiles. m is effectively a measure of the departure of the ray density statistics from Gaussian (c=1). From Figures 1 and 13 it follows that as the profile becomes flatter/more gently undulating m increases (m = 6 for Huntingdonshire and 1.6 for Painscastle) and so may consequently be regarded as some measure of the surface texture. It is therefore of interest to investigate the effect of reducing the illuminated length of the profile. Not only will this enhance the non-Gaussian effects, but it also corresponds to the situation encountered in SAR. The enhanced non-Gaussian effects will naturally become increasingly significant as the illuminated length becomes comparable to, or less than the surface correlation length[19].

6 EFFECT OF VARYING THE ILLUMINATED LENGTH

As the illuminated length L was varied the ray-density probability distributions and their corresponding moments could still be approximately fitted to a Gamma distribution. Figure 14 shows the results for Painscastle with L = 1 km. As before the actual fluctuations are somewhat less than those predicted on the basis of determining m from the second normalised moment. The very different form of the probability distribution to those obtained using very large values of L is immediately apparent, as are the much larger values of $<R^n>/<R>^n$. The actual value of m determined from the second normalised moment decreased with decreasing value of L as expected (situation becoming more non-gaussian). Figure 15 shows the variation of $\{<R^2>/<R>^2 - 1\}$ with L on a logarithmic plot for the four profiles previously studied. The resulting straight lines indicate a power law behaviour with the power index in the range -0.08 to -0.5. This should be contrasted with the predictions of a simple facet model with uncorrelated facets[20] which predicts that $(<R^2>/<R^2> - 1)$ is inversely proportional to L. The discrepancy between the predictions of this model and the results obtained here is due to the existence of large scale surface height (and surface slope) correlations. That is, unless

the profile is approximated by very large facets the adjacent ones are not uncorrelated.

To illustrate the factors determining both the magnitude and the slope of the curves shown in Figure 15 attention can be focussed on the Painscastle profile; modifications to it were made to progressively change it from its original form into one consisting of large flat facets. Figure 16a shows the original profile. Figure 16b shows a smoothed version of it. Figure 16c shows the profile generated by reading the original profile height every 0.25 km and joining the measured values by straight lines. Finally Figure 16d is similar to Figure 16c but the height was read every 1 km. The resulting variation of $(\langle R^2 \rangle / \langle R \rangle^2 - 1)$ with illuminated length is shown in Figure 17. The effect of replacing the original profile by large (1 km) facets is seen to be that the magnitude of the slope of the curves is increased from 0.3 to 1.0, the value expected for a surface composed of uncorrelated facets; the surface slope autocorrelation length ~ 900 m. To further illustrate the influence of surface texture on the scattered ray density statistics Figure 18 shows the variation of the mean ray density $\langle R \rangle$ on illuminated length for the Painscastle profiles shown in Figure 16. At large illuminated lengths the curves flatten off; the length of the illuminated region is then no longer controlling the ray-density statistics. The length L corresponding to this situation occurs when

$$\ell \sim \left[\frac{z}{L^{v/2}}\right]^{\frac{2}{2-v}} .$$

Again the slope of the curve tends to unity as the profile is approximated by large, and hence uncorrelated facets. That is, in the limit of uncorrelated facets the mean ray density is proportional to the number of facets pointing towards the detector, ie $\langle R \rangle$ is proportional to the illuminated length.

When there is large scale surface correlation the slope distribution of the profiles is of paramount importance in determining the magnitude of $\langle R \rangle$. Figure 19 shows histograms of the measured slope distributions for the Painscastle profiles. In each case

the results were symmetrical about $\theta = 0$, where θ is the angle between the vertical axis and a normal to the profile. Although limited in accuracy because of both the difficulty of manually reading the profile slope and the limited number of data points (for the histograms shown the number of slopes measured per profile varied from a low of 75 to a high of 300), they nevertheless show that the value of <R> measured in Figure 18 is related to the probability of a small value of slope. For example the original profile has $P(\theta = 0\text{-}10^{\circ}) \simeq 0.24$ and the highest value of <R>. The next highest is the smoothed curve ($P(0\text{-}10^{\circ}) \simeq 0.22$), followed by the profile read every 0.25 km and joined by straight lines ($P(0\text{-}10^{\circ}) \simeq 0.16$) and finally the large facet case with $P(0\text{-}10^{\circ}) \simeq 0.13$. This is illustrated graphically in Figure 20 where the measured mean ray density is plotted against the measured probability of finding θ between zero and ten degrees for three different illuminated lengths. Also shown is a dotted line of unity slope passing through the origin. Although there are only three points per curve, they do suggest that <R> is proportional to the probability of finding a slope pointing in that direction.

Similar findings to those shown for the modified Painscastle profiles are found for the original four profiles from the four different areas of Britain, and whose normalised second ray density moments are shown in Figure 15. The corresponding variation of <R> with L is shown in Figure 21 and their slope histograms in Figure 22. Again the magnitude of the curves are related to the probability of finding a small slope; both the Hook Bank and Huntingdon profiles have very large values of $P(|\theta| = 0\text{-}10^{\circ})$. As with the modified Painscastle data it is difficult to model the variation of $P(\theta)$ with angle in a consistent manner; there are wide variations in its shape from region to region, a large proportion of which is undoubtedly real and not an artefact of the poor statistics. It is worth noting however that there always appears to be a large probability of finding low values of slope ie there is a high probability of finding near horizontal terrain. Although obvious from everyday experience, it should not be overlooked when modelling land surfaces.

7 CONCLUSIONS

As stated in the introduction the work reported in this memorandum was initiated with the aim of using crude techniques to look at the viability of modelling natural terrain as fractal surfaces. To that end the results presented here from four different areas of Britain, ranging from the gently undulating terrain of Huntingdonshire to the much more rugged countryside of Wales, do indeed show that, at least to the degree of accuracy attempted here, that they can be realistically modelled either as fractal, or as a hierarchy of different fractals. It is encouraging that similar behaviour has been observed for terrain in the USA. It is also perhaps noteworthy that the power index υ was in the range 1-1.8. It would be interesting to know whether villages, towns and cities could also be realistically represented as fractals, and if so what the typical values of υ may be. This may then be of some use in radar modelling of land surfaces. The (possible) fractal nature of land profiles also has implications for digital mapping in terms of the maximum usable element size. To extend this work further such digital mapping will be necessary to enable both greater accuracy and speed to be achieved.

When the land profiles were smoothed by a crude small scale smoothing the resulting profiles approximated another simple, but relatively well characterised model, the sub-fractal surface. In practice the transition from fractal to sub-fractal behaviour is probably relatively smooth. The actual mechanism of smoothing could in practice arise from either the finite bandwidth of the radiation, the effect of using a relatively long wavelength compared to the high frequency surface components or where spatial or temporal averaging of interference occurs in the detection system. Whatever the mechanism, the adoption of a sub-fractal model allows rays to be drawn from the surface. The resulting ray-density statistics are in broad agreement with theory[3,15,16] although considerably more work using digital maps and computer graphics needs to be carried out to verify the fine details. For example, in the Fresnel region it is predicted by Jakeman[3,16] that the second normalised ray density moment is directly realted to υ; a measurement of $\langle R^2 \rangle / \langle R \rangle^2$ would therefore allow υ to be determined. Because of the

uncertainty of whether a Fresnel or Fraunhofer approximation, or indeed if either one is relevant for the data in this memorandum, and the limited accuracy/resolution achieved, and the somewhat arbitrary smoothing used, these predictions could not be confirmed. Also more work is needed to clarify the form of the ray density autocorrelation function; the correlations existing within the data contain much of the texture information. An obvious extension of this work would be to study the effect of shadowing/multiple scattering.

In spite of the limitations of this work the fact that the ray density distribution is a reasonable approximation to a Gamma function is of significance, as precisely this distribution is assumed when representing the underlying cross-section fluctuations of the land or sea-bed when modelling SAR and sonar imaging. A Gamma-distributed surface cross-section fluctuation can be shown[21] to arise from a diffusion process, giving scatterer migration coupled with local sources and sinks of scatterers, analogously to the process of birth and death. Phenomenologically therefore Gamma distributions may possibly be expected to apply whenever small scale surface roughness is modulated by large scale sizes.

Although the variation of mean scattered intensity $<I(\theta)>$ with angle is a sensitive function of the fractal parameters υ and L, the inverse problem of determining υ and L from measurements of the variation of $<I(\theta)>$ with angle is not in general feasible. Consequently some other method of determining the surface texture of rough surfaces and which may be applicable to metrology is needed. To this end the concept of using white light and ray descriptions may have an application. As shown in this memorandum the non-gaussian behaviour of the scattered ray statistics is enhanced by reducing the illuminated region to a size comparable with, or smaller than, the surface height/slope correlation length. It may also be valuable to consider describing rough surfaces not in terms of a fractal model but rather in terms of a surface model that pre-supposes a Gamma-distributed cross-section or scatter number density variation. The surface texture may then possibly be described in terms of the order parameter m in the

Gamma-distribution and the surface autocorrelation function, as is done in SAR modelling.

ACKNOWLEDGEMENTS

The author is extremely grateful for a helpful discussion on SAR modelling from Dr C Oliver and invaluable help and guidance on all aspects of this work from Dr E Jakeman.

REFERENCES

1 Jordan, D L; Hollins, R C; Jakeman, E; 1983, Appl Phys B, 31, 179.

2 Jordan, D L; Hollins, R C; Jakeman, E; 1986, Wear, 109, 127.

3 Jakeman, E; 1982, J Opt Soc Am, 72, No 8, 1034.

4 Oliver, C J; 1985, RSRE Memorandum 3775.

5 Oliver, C J; 1986, Inverse Problems, 2, 481.

6 Oliver, C J; Tough, R J A; 1986, Optica Acta, 33, No 3, 223.

7 Oliver, C J; 1988, Inverse Problems, 4, 843.

8 Sayles, R S; Thomas, T R; 1978, Nature, 271, 431.

9 Berry, M V; 1979, J Phys A, 12, 781.

10 Mark, D M; Aronson, P B; 1984, Math Geology, 16, No 7, 671.

11 Jordan, D L; Hollins, R C; Jakeman, E; Prewett, A; 1988, Surface Topography, 1, 27.

12 Beckmann, P; Spizzichino, A; The scattering of electromagnetic waves from rough surfaces, Pergamon Press, Oxford, 1963.

13 Berry, M V; 1977, J Phys A, 10, 2061.

14 Berry, M V; Upstill, C; Progress in Optics XIII (North-Holland, Amsterdam, 1980) 258.

15 Jakeman, E; 1982, J Phys A, 15, L55.

16 Jakeman, E; 1987, AGARD Conf Proc 419, Scattering and Propagation in Random Media, 13-1.

17 Jakeman, E; 1983, Optica Acta, 30, No 9, 1207.

18 Jakeman, E; Jefferson, J H; 1984, Optica Acta, 31, No 8, 853.

19 Oliver, C J; 1984, Optica Acta, 31, No 6, 701.

20 Jakeman, E; Pusey, P N; 1974, RSRE Memorandum 2874.

21 Jakeman, E; 1980, Optica Acta, 27, 735.

FIGURE CAPTIONS

Figure 1(a) Hook Bank - Elmley Castle (E-W) profile
(b) Huntingdonshire (N-S) profile
(c) Dartmoor profile
(d) Painscastle (E-W)

Figure 2 Structure function of land profiles

Figure 3(a) Profile consisting of a sum of sinusoids
(b) Structure function of profile shown in Figure 3a

Figure 4(a) Smoothed Dartmoor profile
(b) Dartmoor profile with only the dominant structures retained

Figure 5 Structure functions corresponding to original Dartmoor profile, smoothed profile (Figure 4a) and profile with dominant structures only (Figure 4b).

Figure 6 Surface height autocorrelation functions corresponding to profiles shown in Figure 1.

Figure 7 Normalised mean scattered intensity as a function of scattering angle.

Figure 8 Ray density results for Hook Bank - Elmley Castle profile
(a) Normalised moments
(b) Probability distribution
(c) Normalised autocorrelation function

Figure 9 Ray density results for Huntingdonshire (N-S)
(a) Normalised moments
(b) Probability distribution
(c) Normalised autocorrelation data

Figure 10 Ray density results for Painscastle (E-W)

(a) Normalised moments

(b) Probability distribution

(c) Normalised autocorrelation function

Figure 11 Ray density results for Painscastle (E-W)

(a) Contrast versus detector size

(b) Contrast versus detector height above surface (detector size = 2 cm)

Figure 12 Ray density results for Dartmoor

(a) Normalised moments

(b) Probability distribution

(c) Normalised autocorrelation function at a height of 740 m

Figure 13 C^2 versus 1/m illustrating the range of values obtained from the profiles shown in Figure 1

Figure 14 Ray density results for Painscastle with an illuminated length of 1 km

(a) Normalised moments

(b) Probability distribution

Figure 15 $\{<R^2>/<R>^2 - 1\}$ versus illuminated length for the four profiles shown in Figure 1

Figure 16(a) Original Painscastle profile

(b) Smoothed Painscastle profile

(c) Profile obtained by reading the height in (a) every 0.25 km and joining the points by straight lines

(d) Profile obtained by reading the height in (a) every 1 km and joining the points by straight lines

Figure 17 $(<R^2>/<R>^2 - 1)$ versus illuminated length for the profiles shown in Figure 16.

Figure 18 Variation of mean ray density $<R>$ with illuminated length for the profiles shown in Figure 16.

Figure 19 Slope probability distributions for the profiles shown in Figure 16.

Figure 20 Mean ray density versus probability of finding a slope pointing towards detector for profiles shown in Figure 16.

Figure 21 Variation of mean ray density with illuminated length for the original profiles shown in Figure 1.

Figure 22 Slope probability distributions for the original profiles shown in Figure 1.

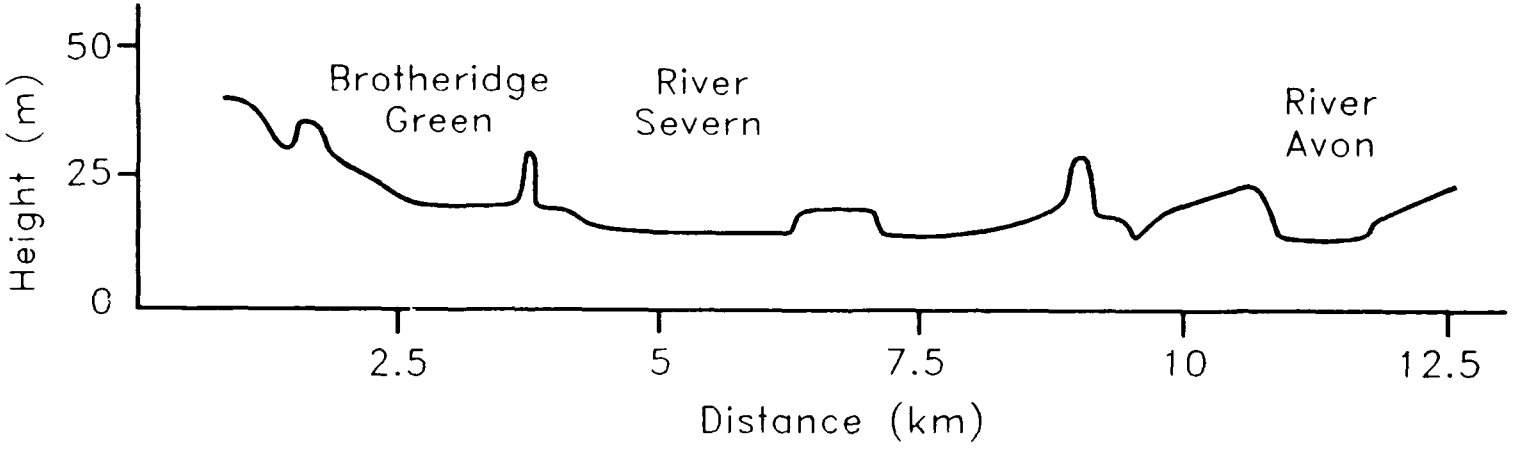
Height (m)
50
25
0
Brotheridge Green
River Severn
River Avon
2.5
5
7.5
10
12.5
Distance (km)

FIGURE 1(a)

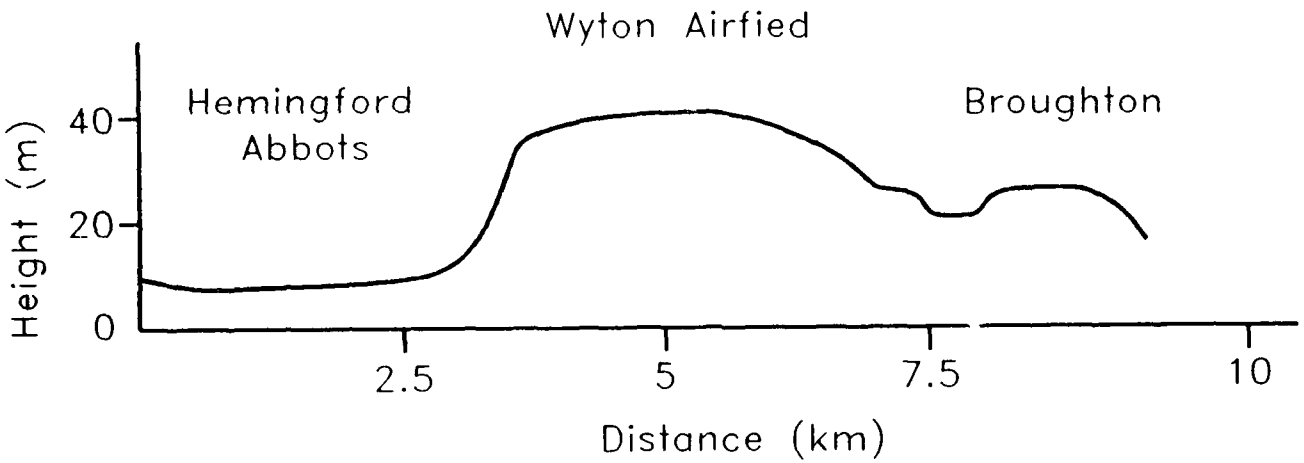
Wyton Airfied
Hemingford
Abbots
Broughton
Height (m)
40
20
0
2.5
5
7.5
10
Distance (km)

FIGURE 1 (b)

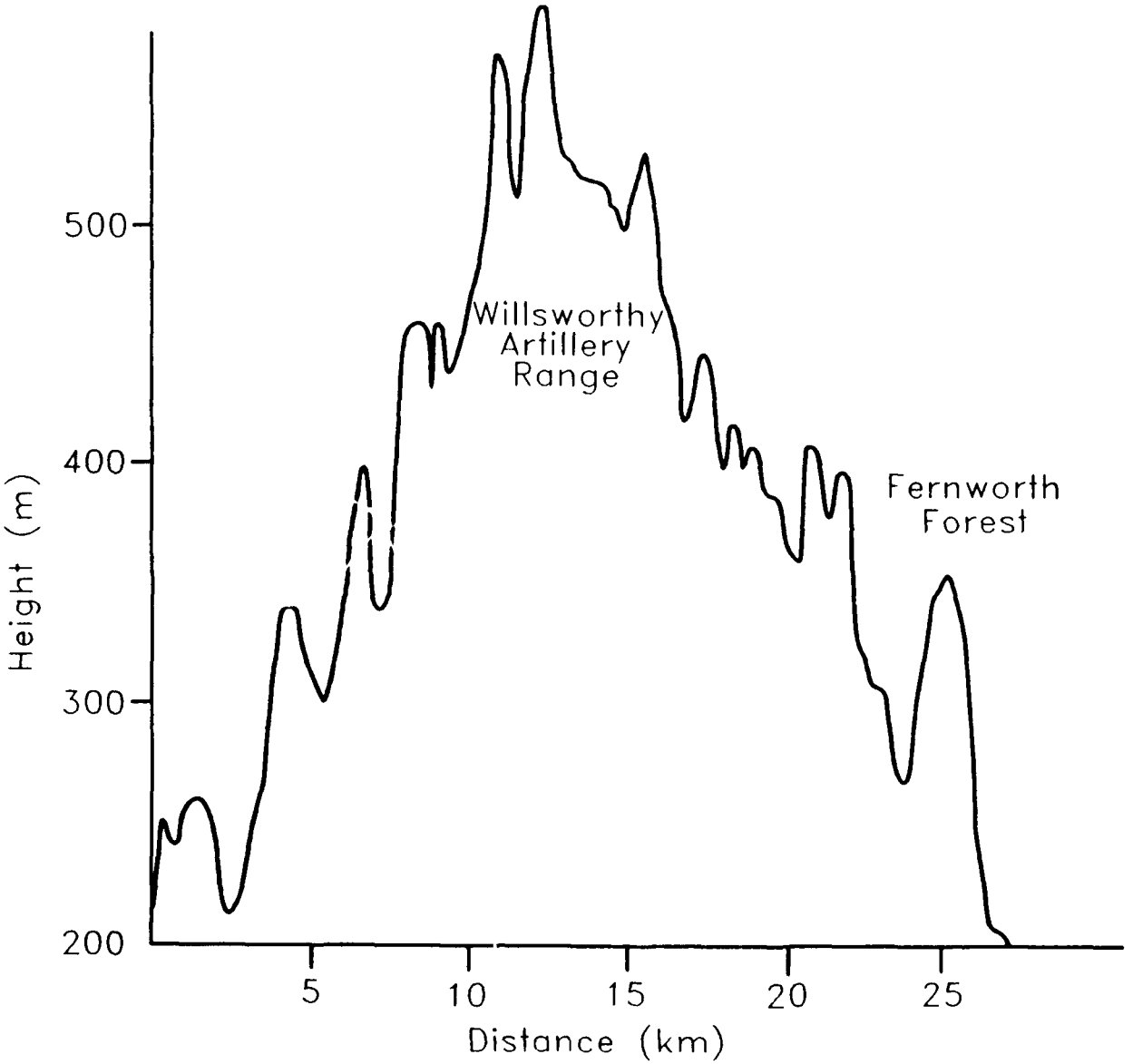
500
400
300
200
Height (m)
Willsworthy
Artillery
Range
Fernworth
Forest
5
10
15
20
25
Distance (km)

FIGURE 1 (c)

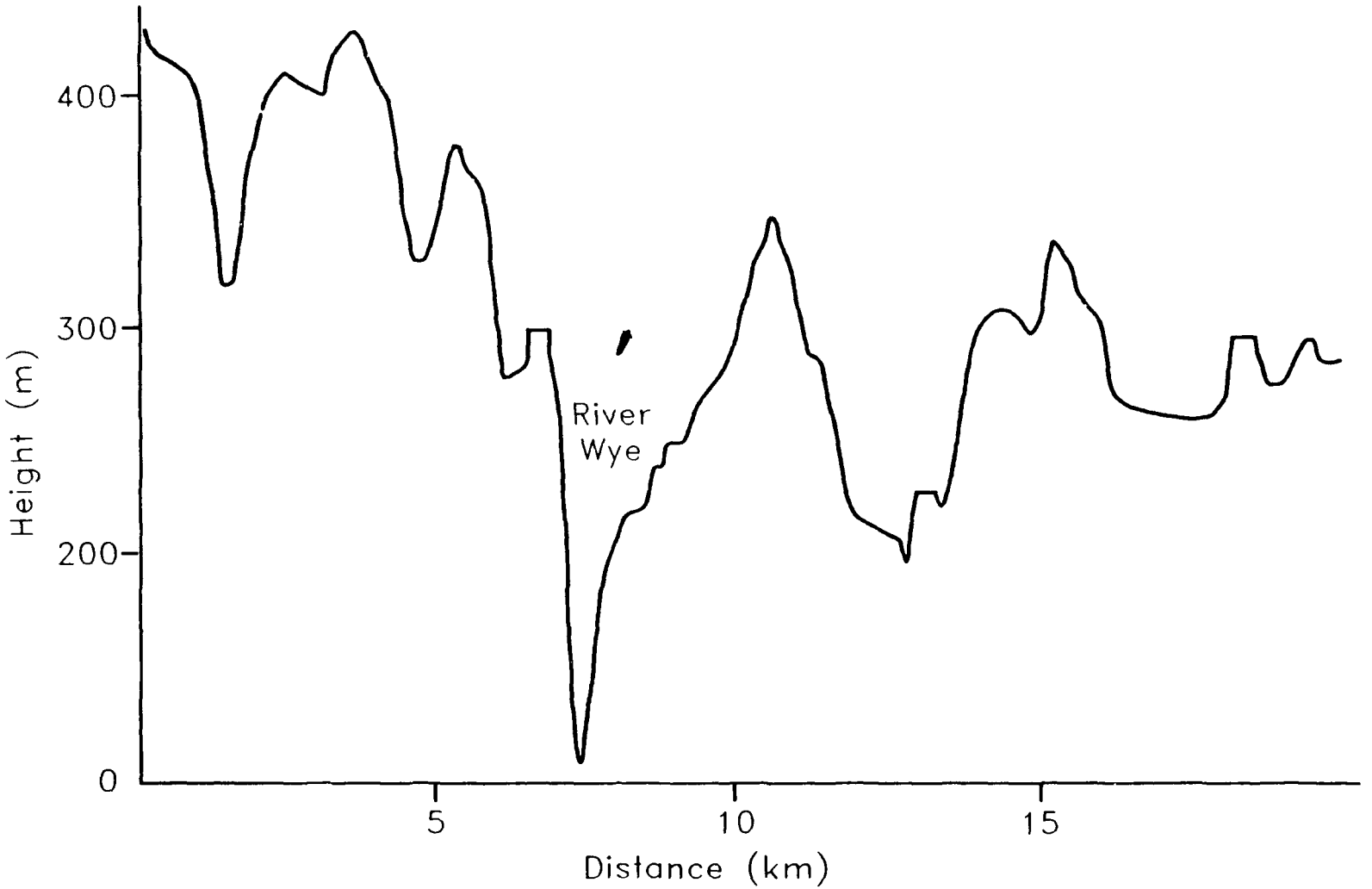

FIGURE 1 (d)

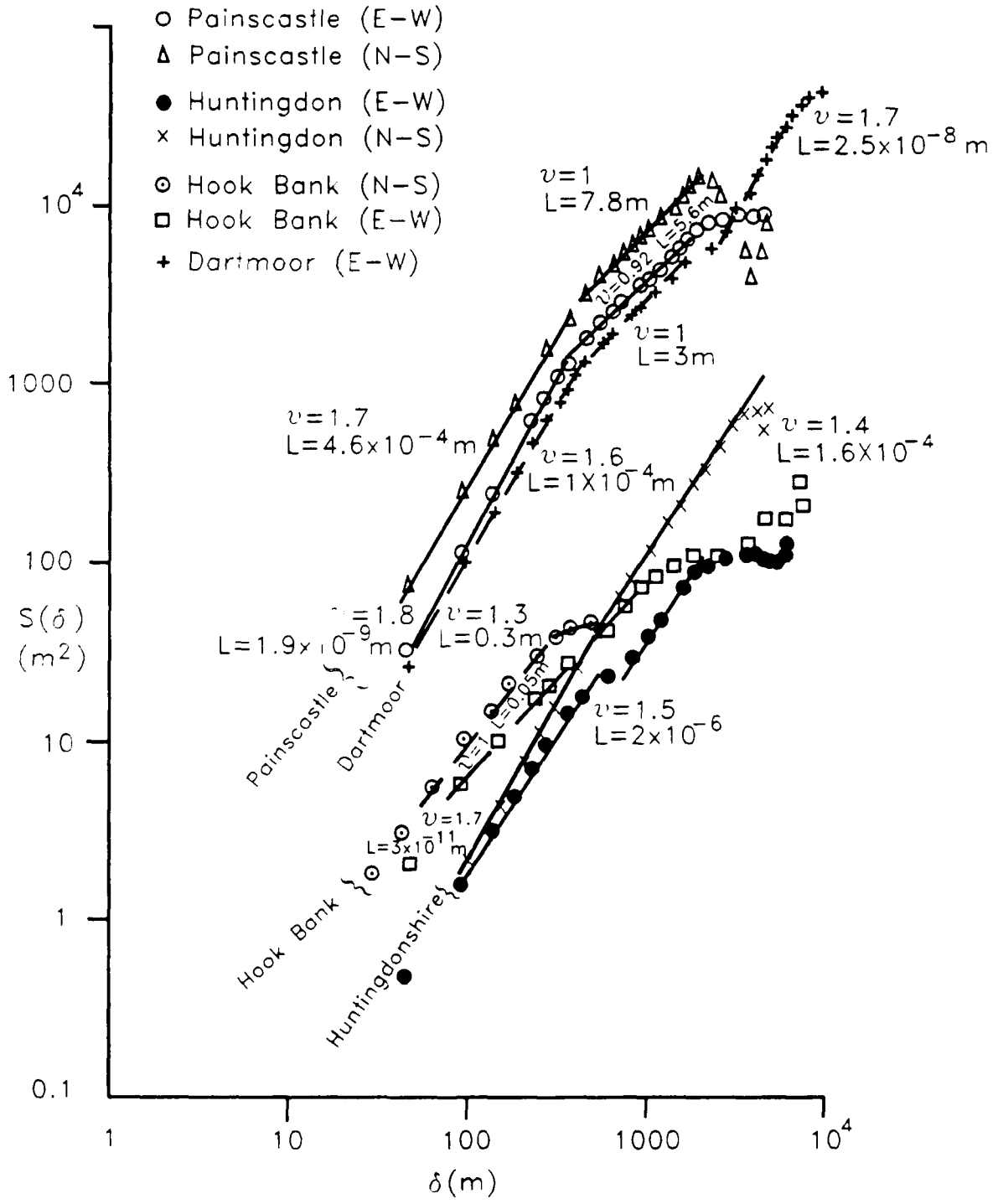
Painscastle (E–W)
Painscastle (N–S)
Huntingdon (E–W)
Huntingdon (N–S)
Hook Bank (N–S)
Hook Bank (E–W)
Dartmoor (E–W)
υ=1.7
L=2.5×10⁻⁸ m
υ=1
L=7.8m
υ=1
L=3m
υ=1.7
L=4.6×10⁻⁴m
υ=1.6
L=1×10⁻⁴m
υ=1.4
L=1.6×10⁻⁴
υ=1.8
L=1.9×10⁻⁹m
υ=1.3
L=0.3m
υ=1.5
L=2×10⁻⁶
υ=1.7
L=3×10⁻¹¹m
Painscastle
Dartmoor
Hook Bank
Huntingdonshire
S(δ)
(m²)
δ(m)
0.1
1
10
100
1000
10⁴

FIGURE 2

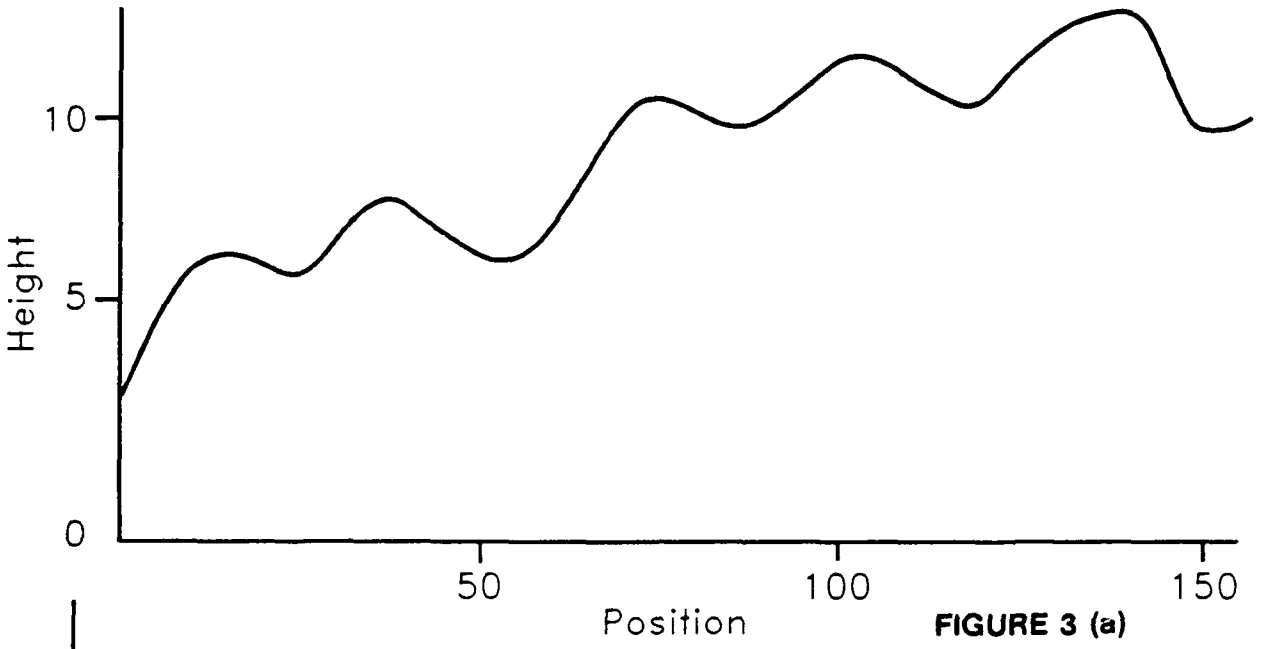

FIGURE 3 (a)

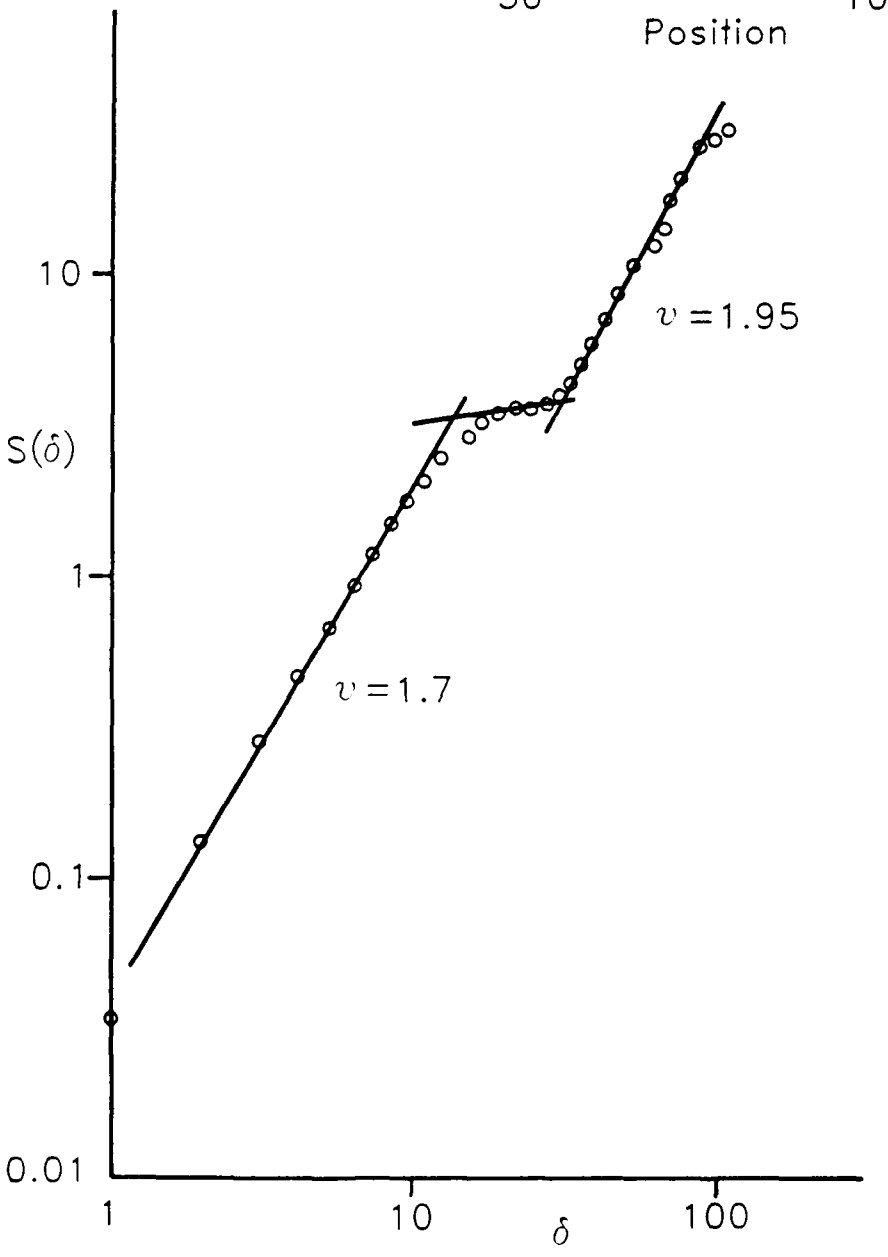

FIGURE 3 (b)

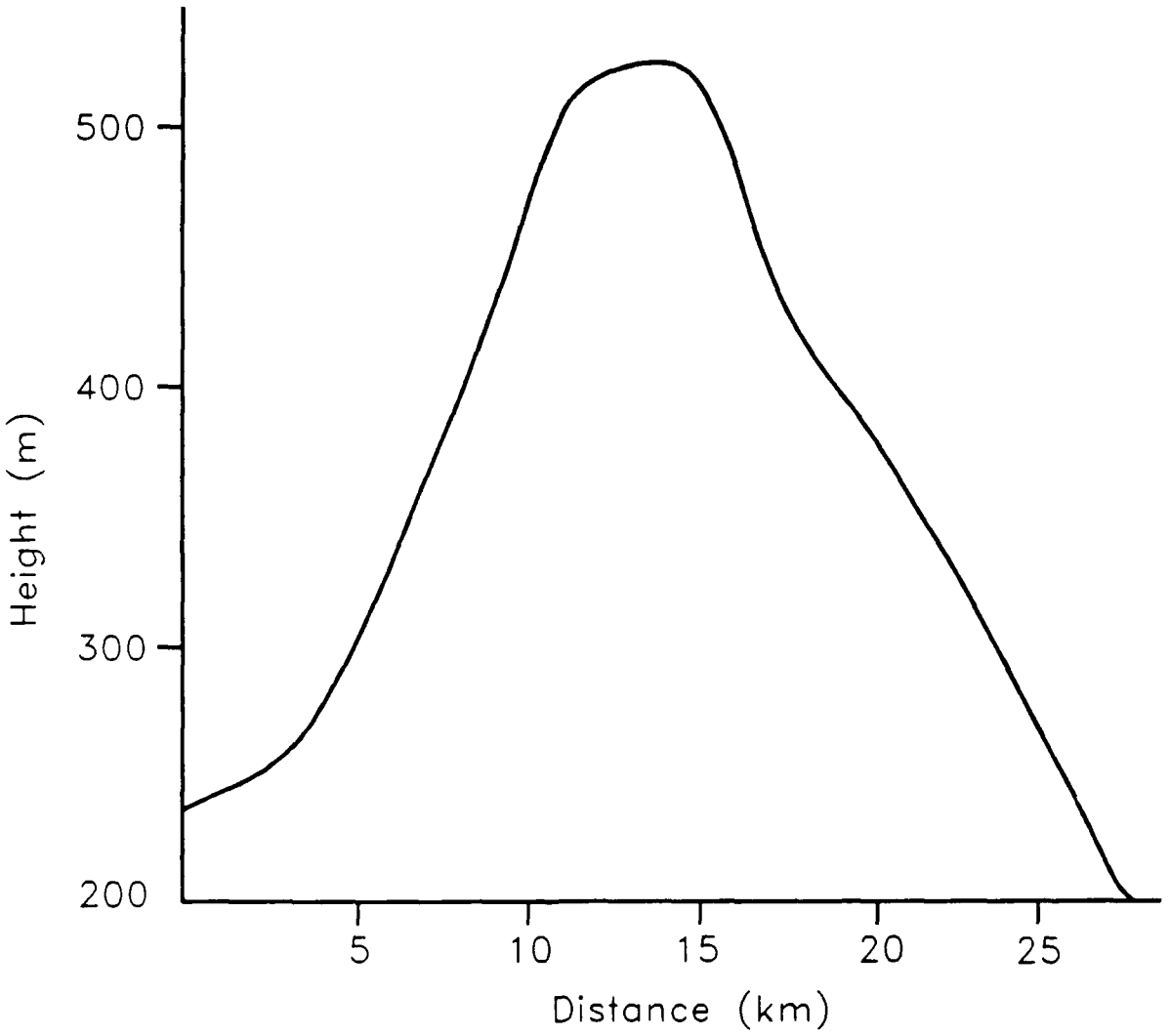

FIGURE 4 (a)

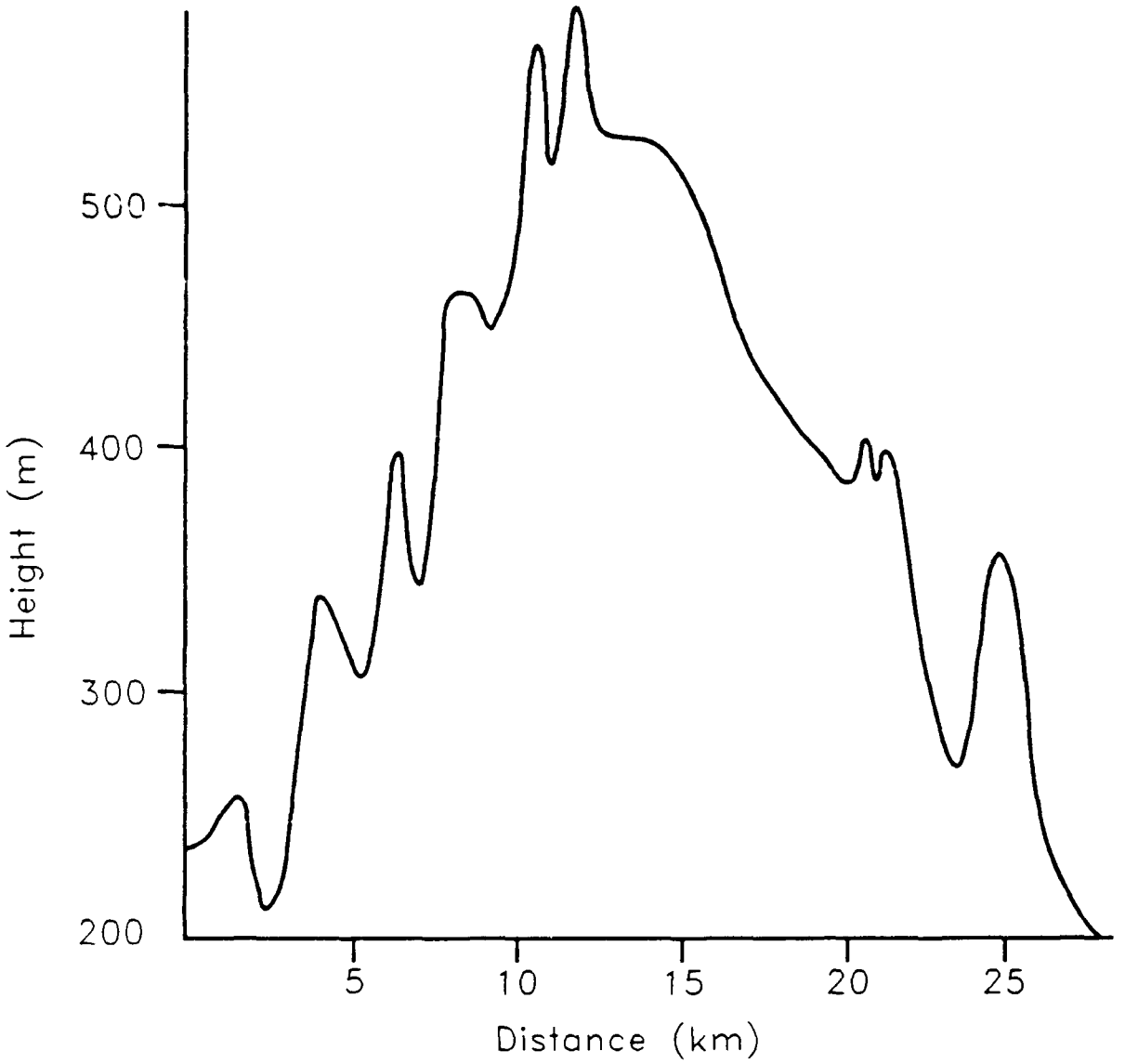

FIGURE 4 (b)

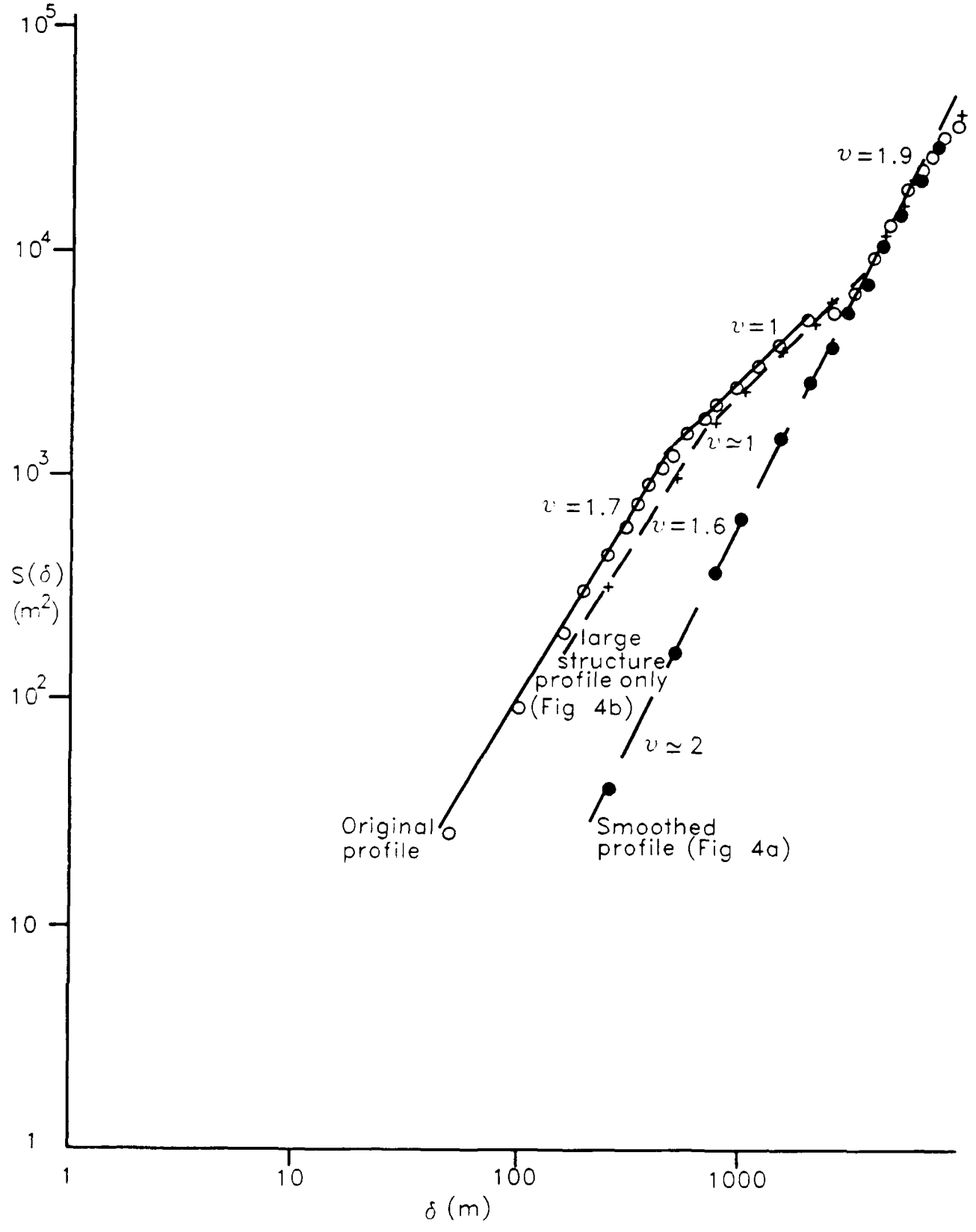
10^5
10^4
10^3
10^2
10
1
S(δ)
(m²)
υ = 1.9
υ = 1
υ ≃ 1
υ = 1.7
υ = 1.6
large
structure
profile only
(Fig 4b)
υ ≃ 2
Original
profile
Smoothed
profile (Fig 4a)
1
10
100
1000
δ (m)

FIGURE 5

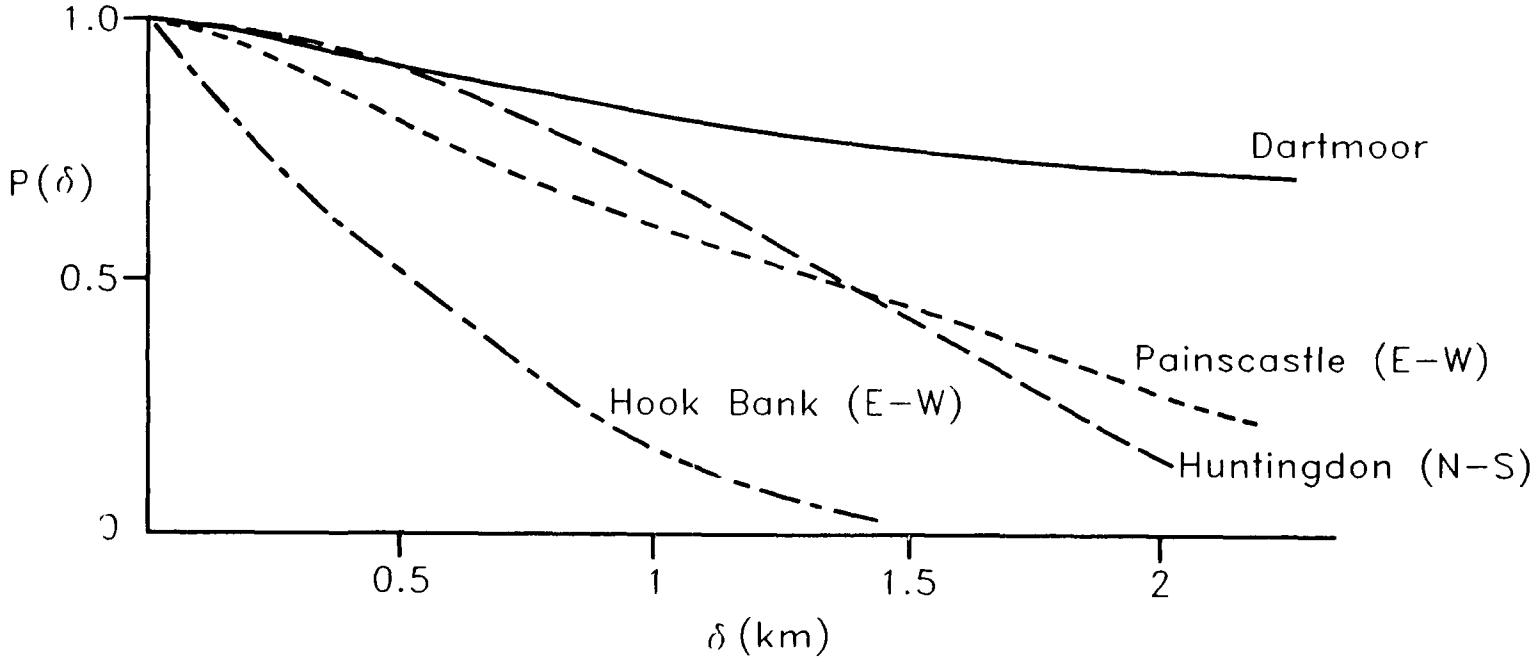
1.0
P(δ)
0.5
0
Dartmoor
Painscastle (E–W)
Hook Bank (E–W)
Huntingdon (N–S)
0.5
1
1.5
2
δ (km)

FIGURE 6

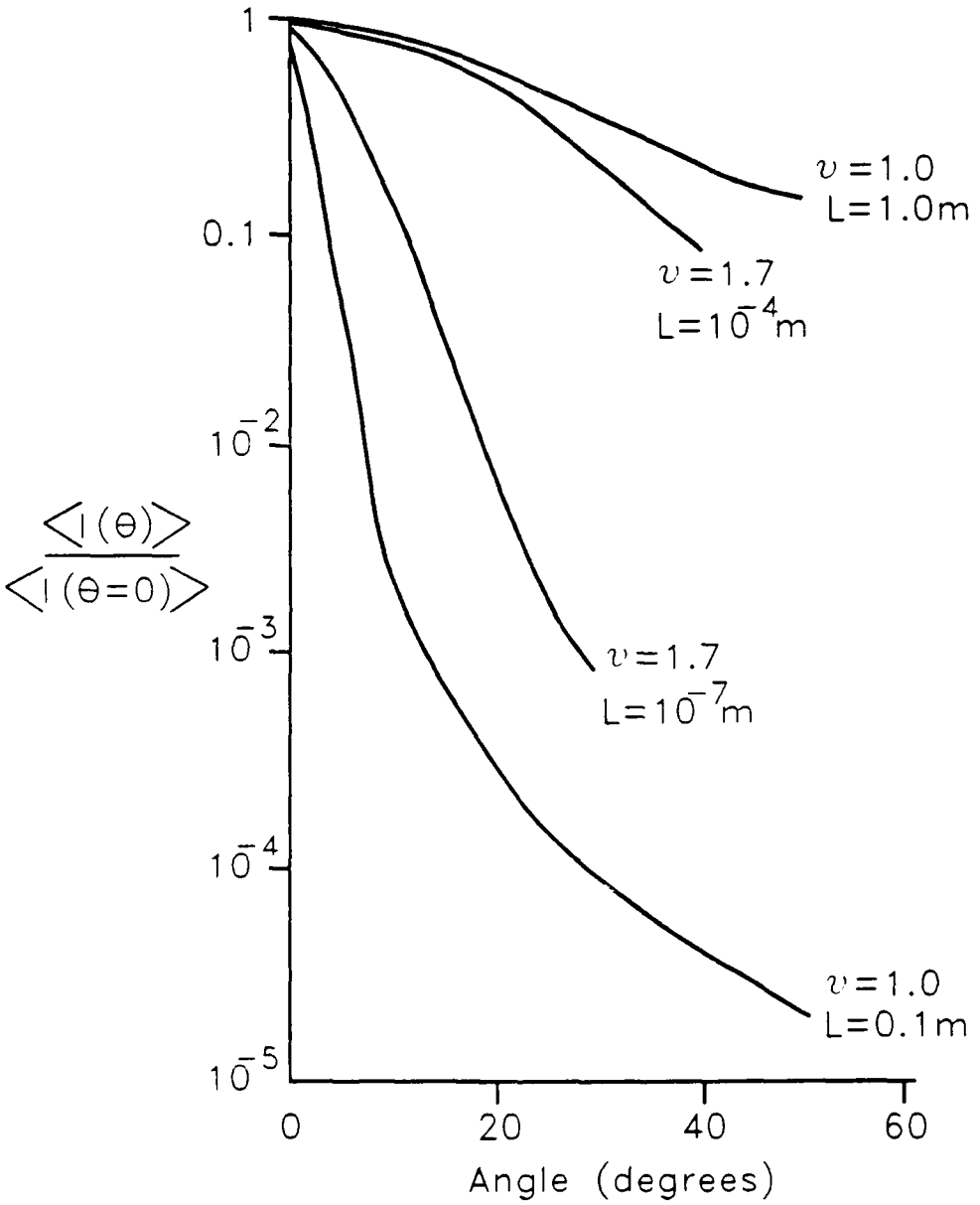
1
0.1
10^{-2}
10^{-3}
10^{-4}
10^{-5}
$\frac{\langle I(\theta)\rangle}{\langle I(\theta=0)\rangle}$
$v=1.0$
L=1.0m
$v=1.7$
$L=10^{-4}$m
$v=1.7$
$L=10^{-7}$m
$v=1.0$
L=0.1m
0
20
40
60
Angle (degrees)

FIGURE 7

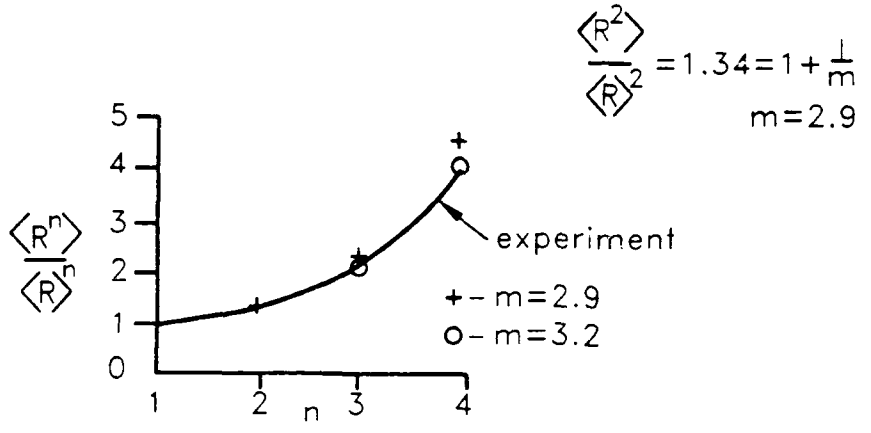

FIGURE 8 (a)

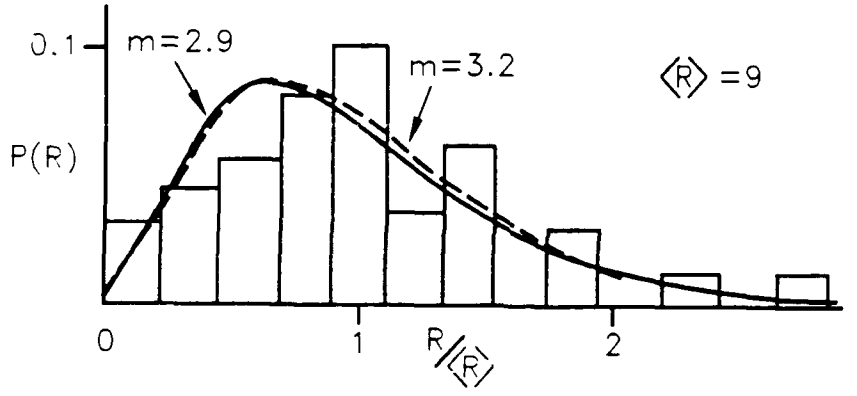

FIGURE 8 (b)

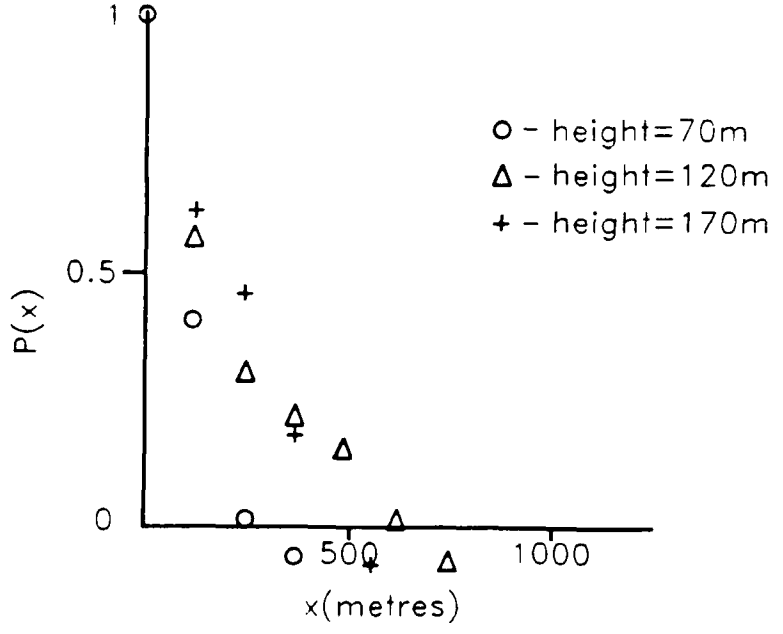

FIGURE 8 (c)

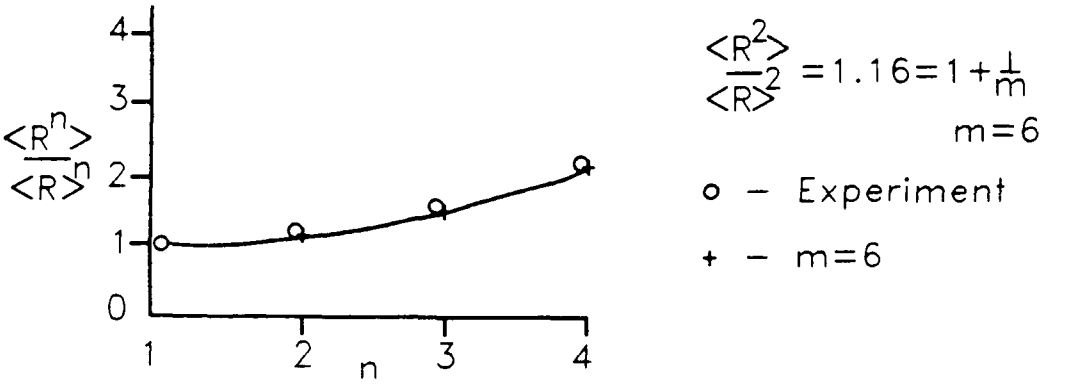

FIGURE 9 (a)

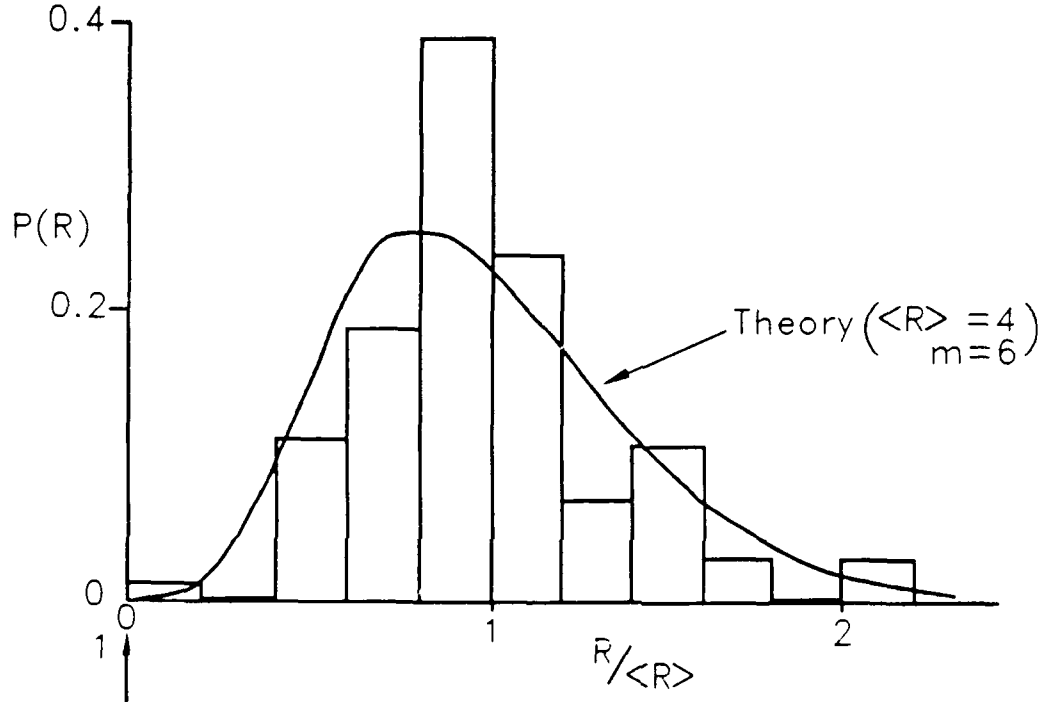

FIGURE 9 (b)

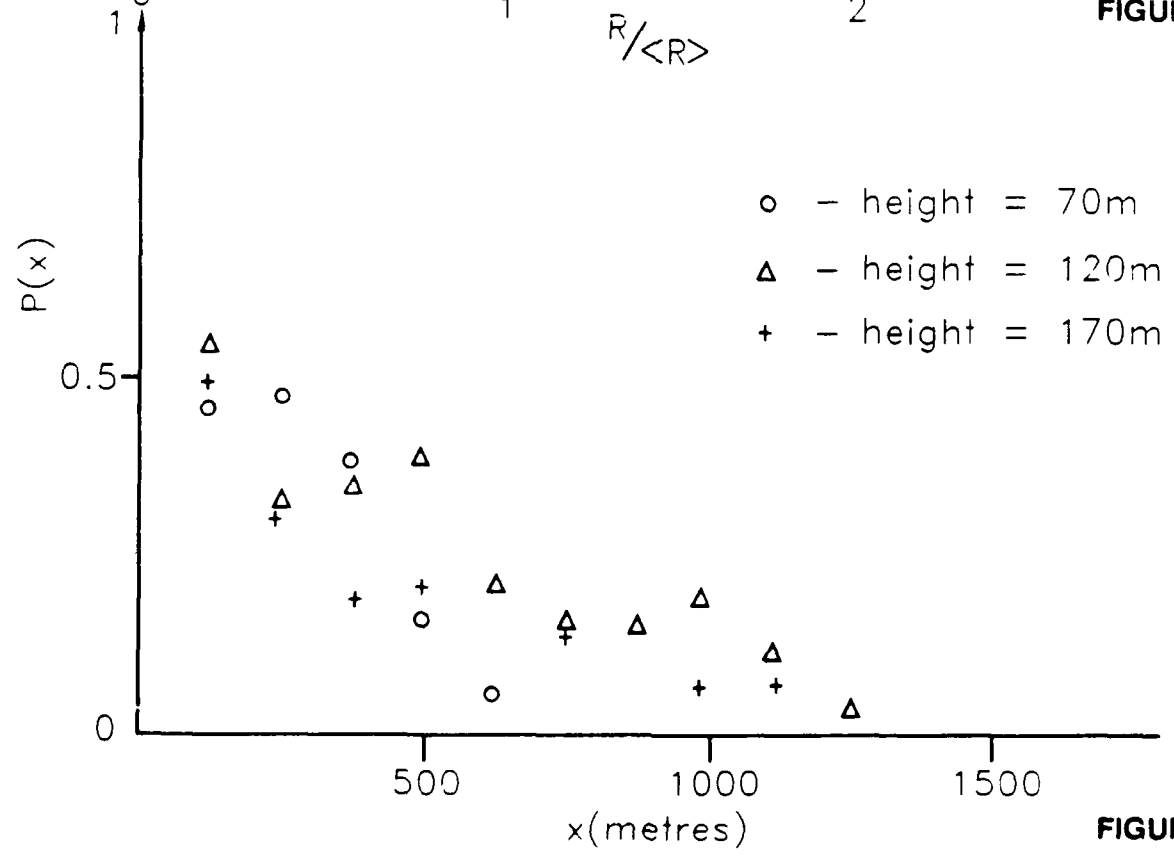

FIGURE 9 (c)

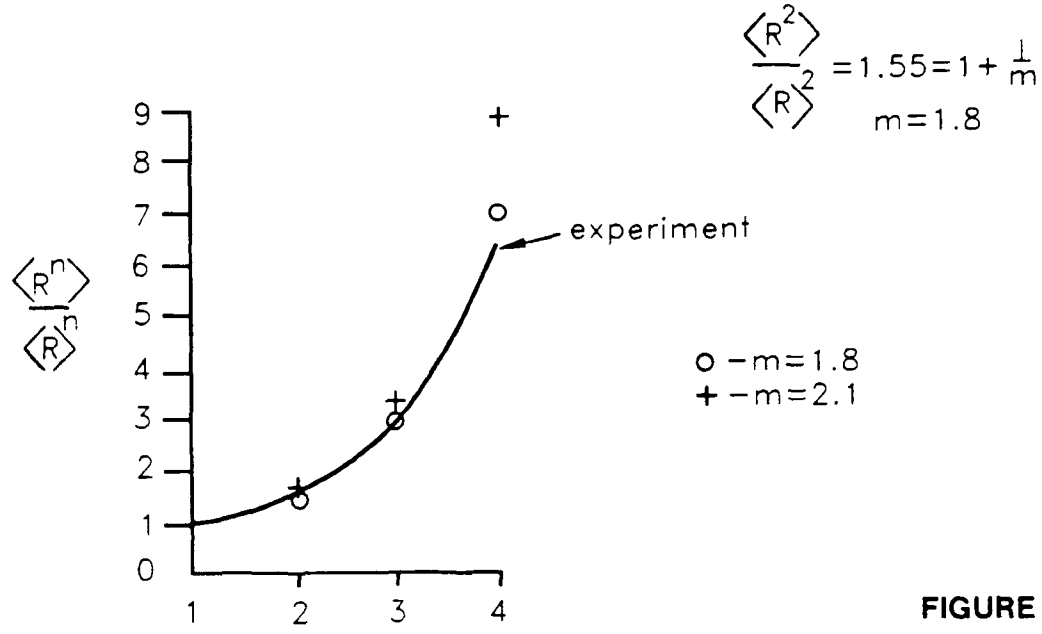

FIGURE 10 (a)

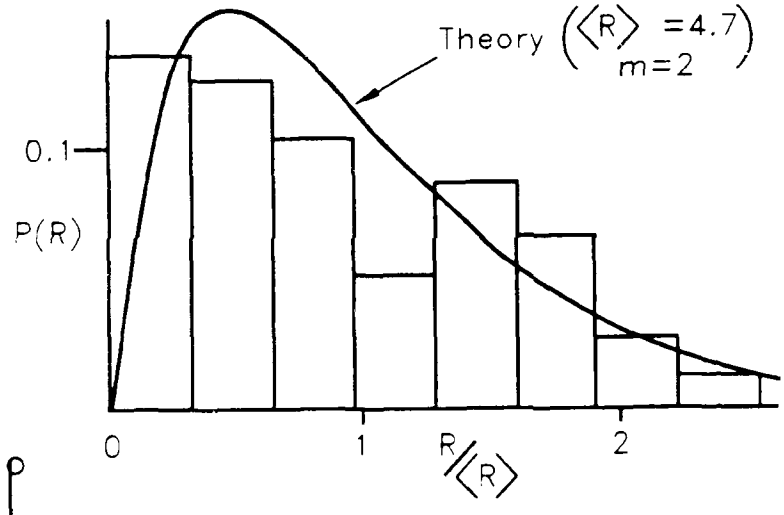

FIGURE 10 (b)

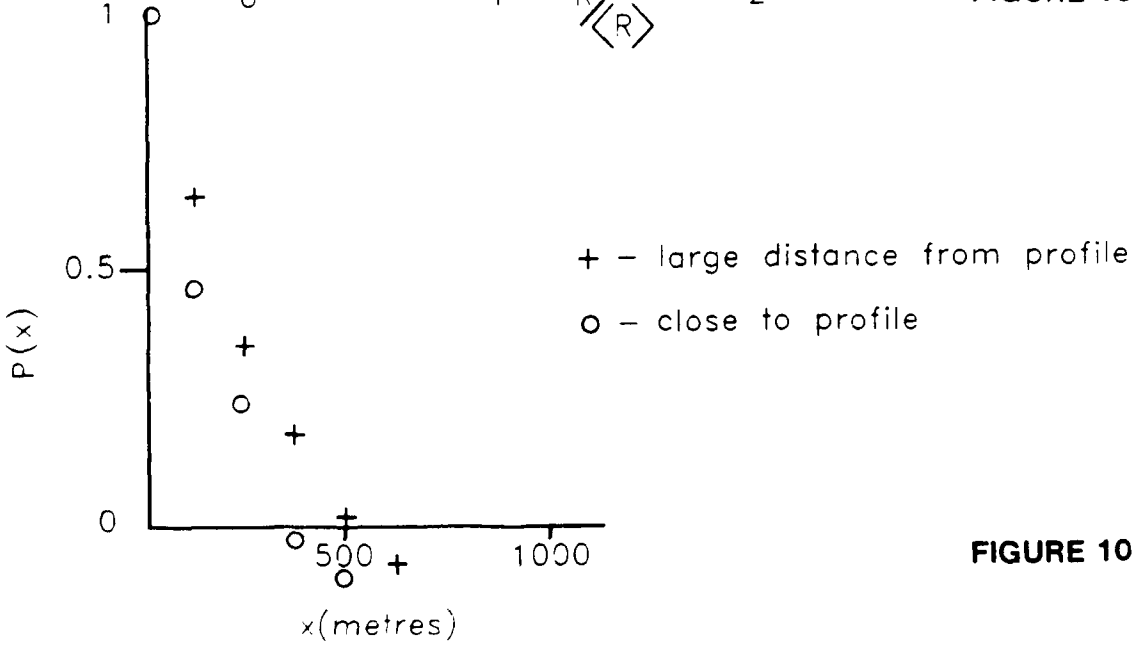

FIGURE 10 (c)

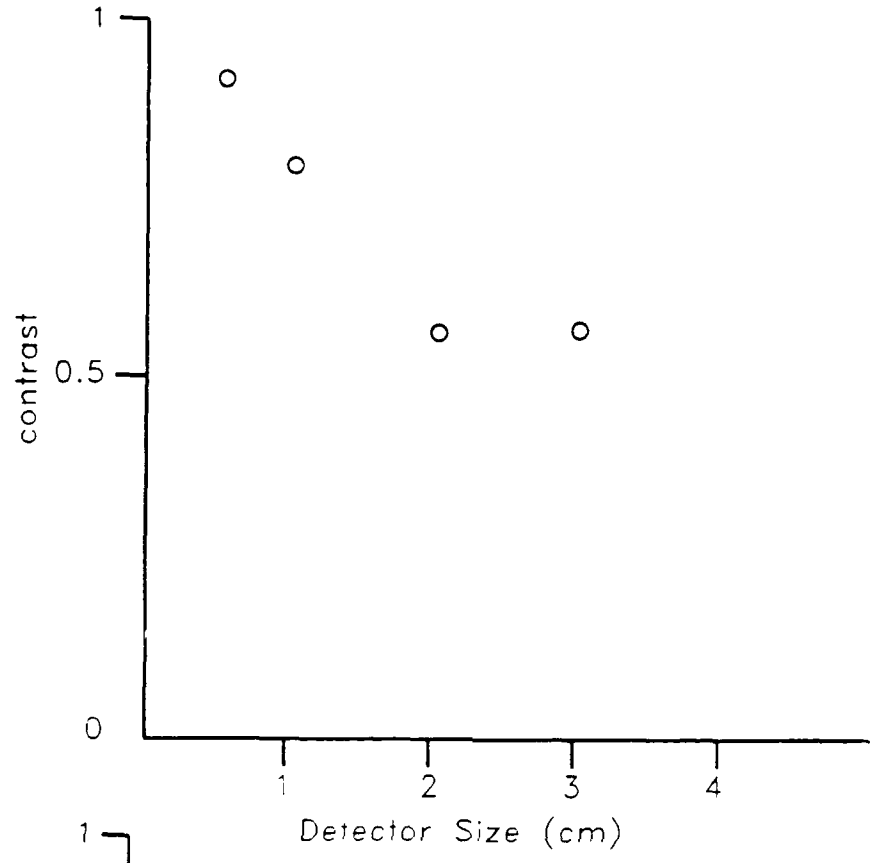

FIGURE 11 (a)

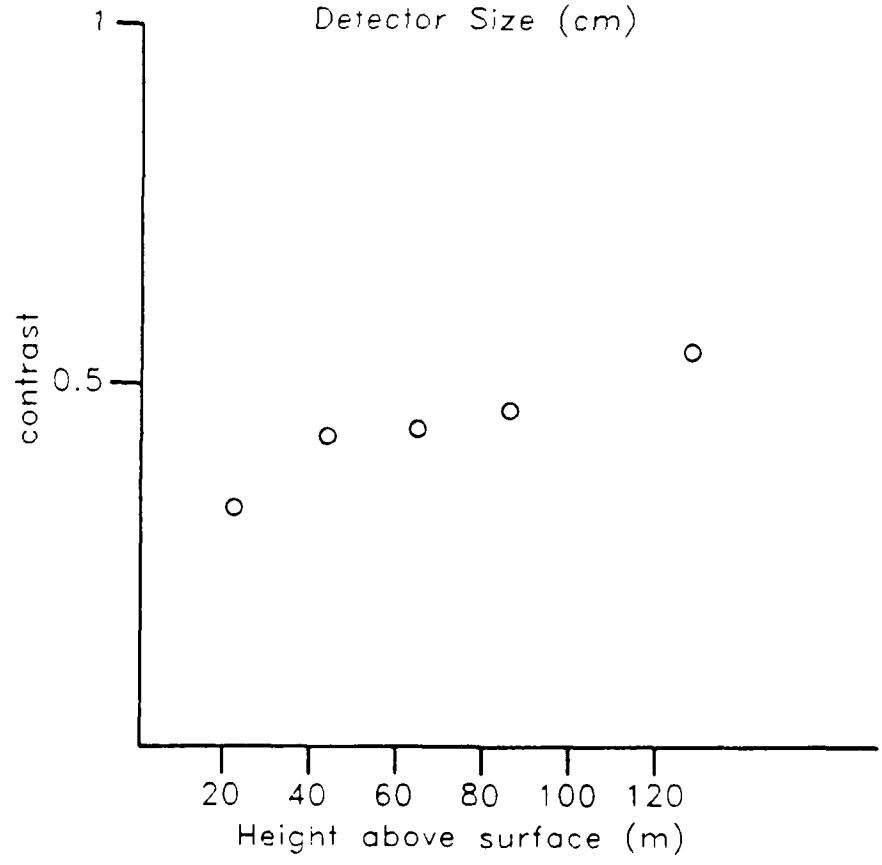

FIGURE 11 (b)

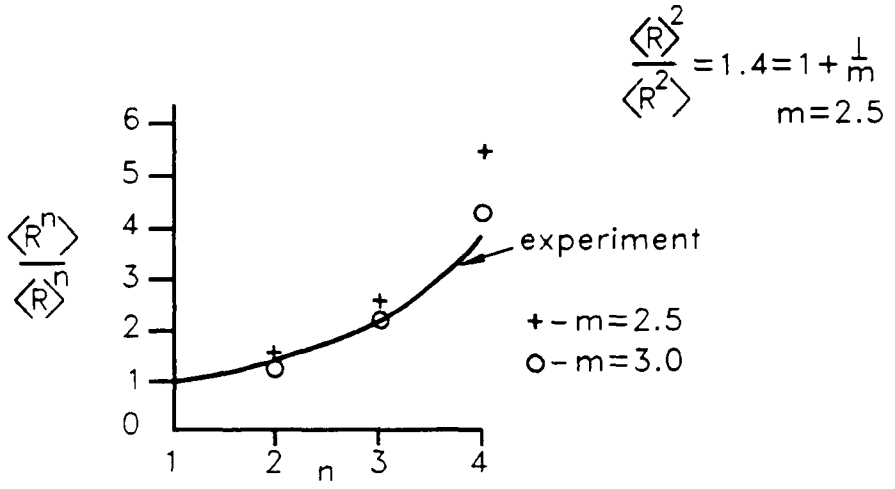

FIGURE 12 (a)

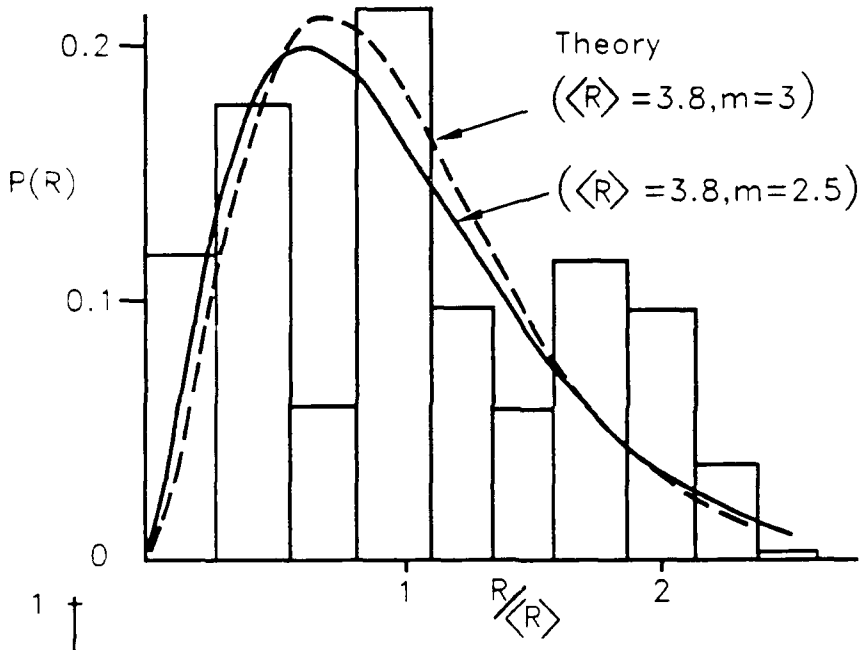

FIGURE 12 (b)

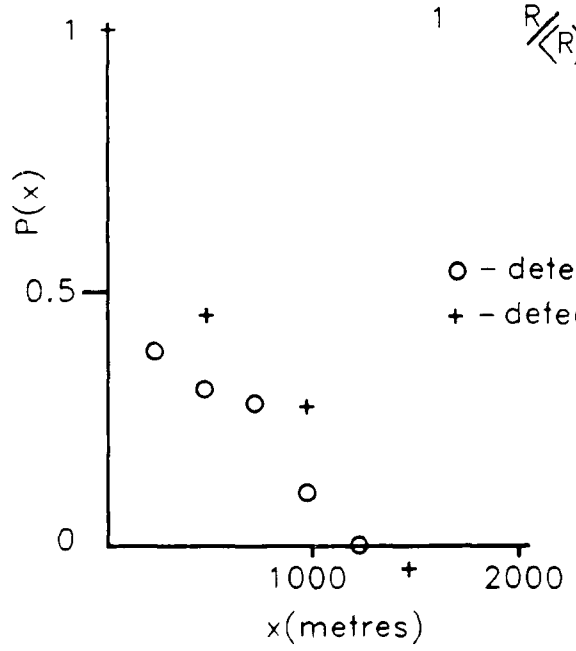

FIGURE 12 (c)

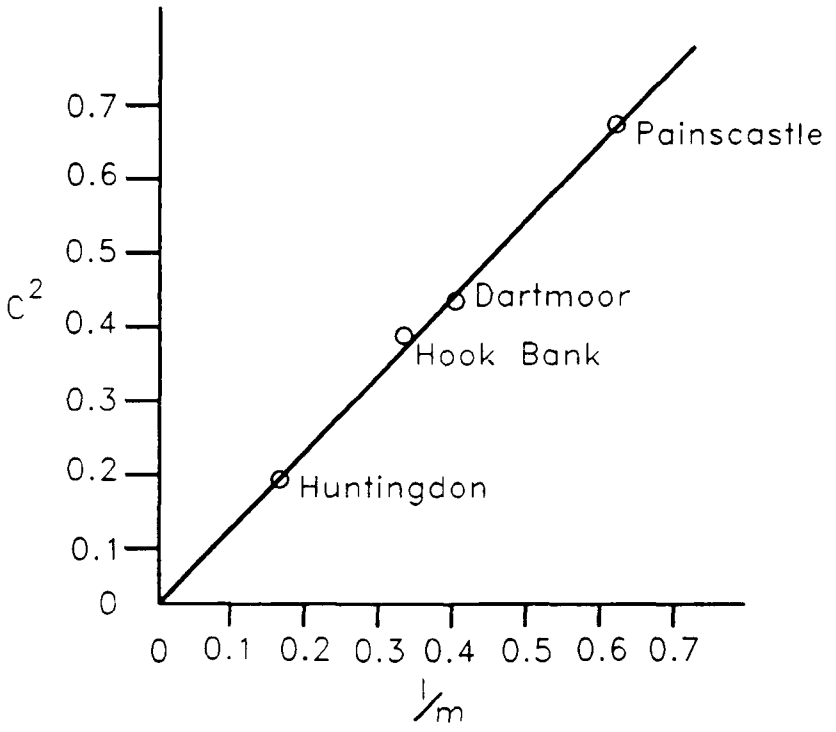
0.7
0.6
0.5
C^2
0.4
0.3
0.2
0.1
0
Painscastle
Dartmoor
Hook Bank
Huntingdon
0 0.1 0.2 0.3 0.4 0.5 0.6 0.7
1/m

FIGURE 13

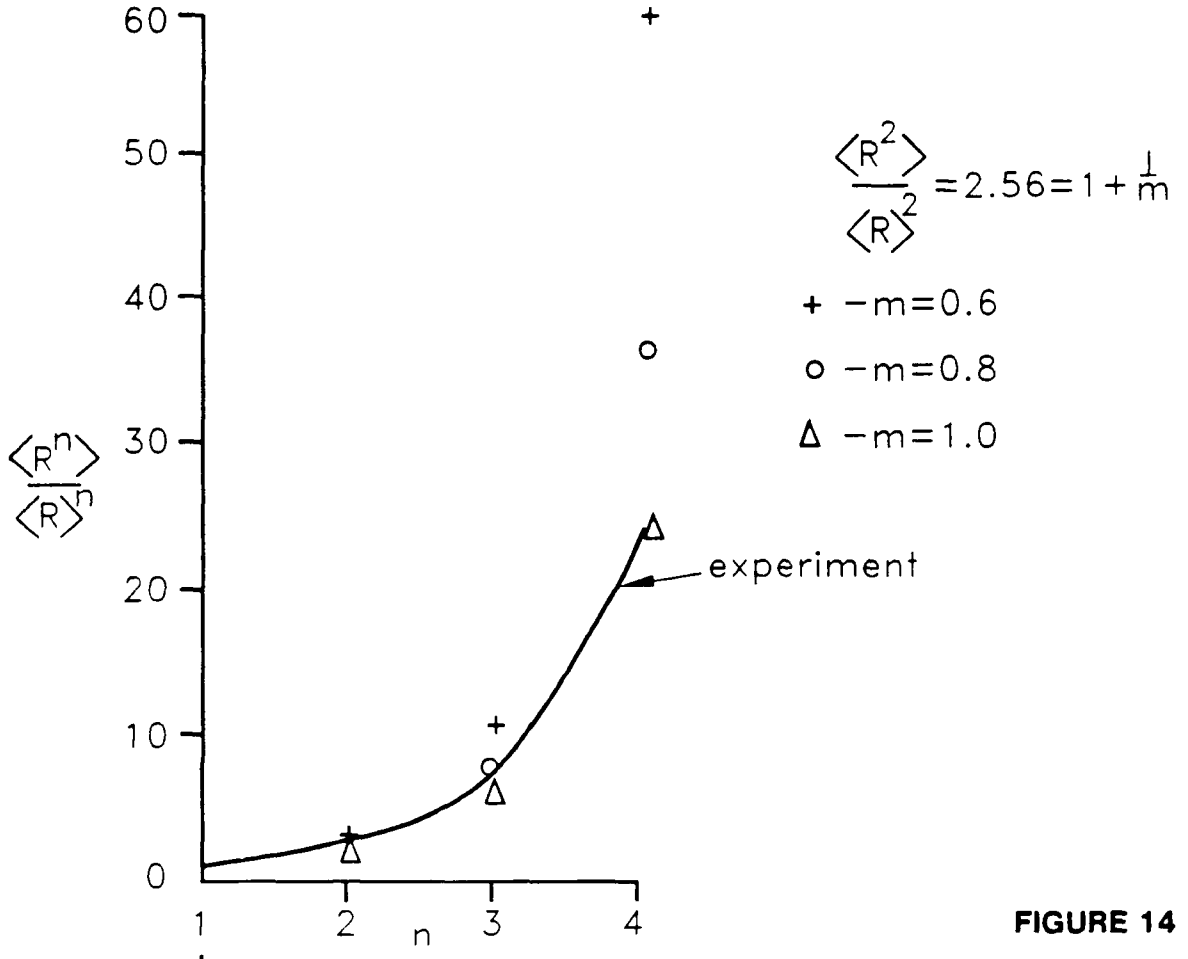

FIGURE 14 (a)

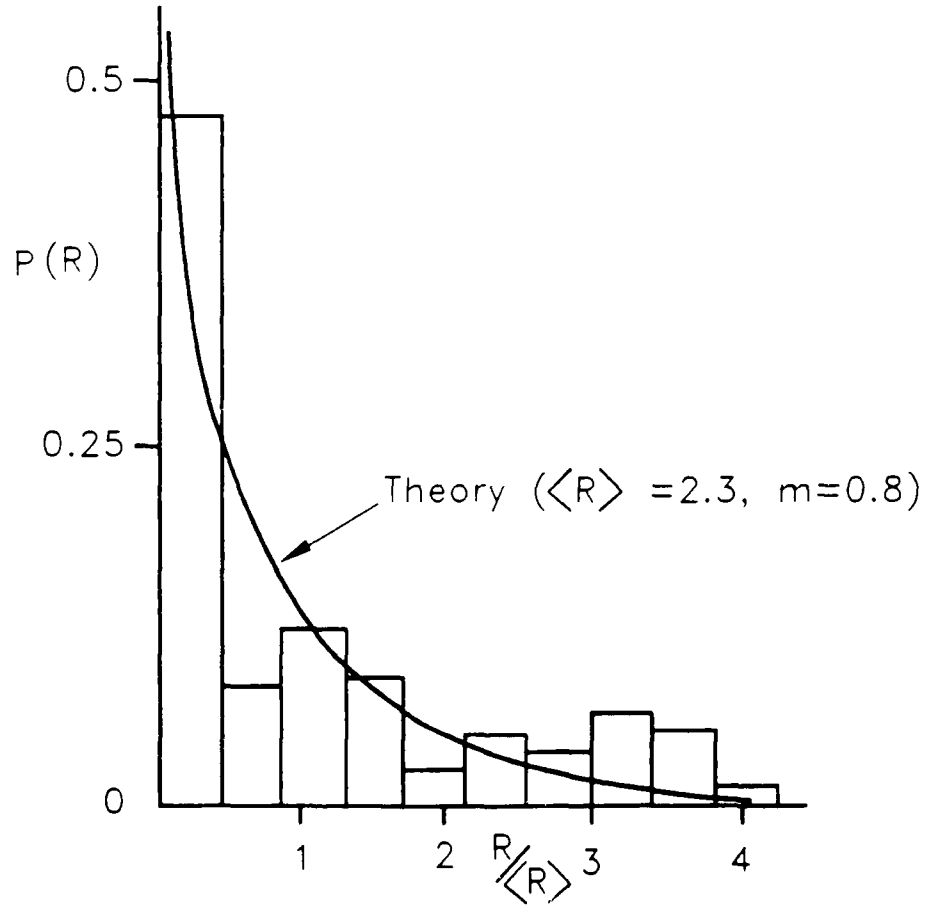

FIGURE 14 (b)

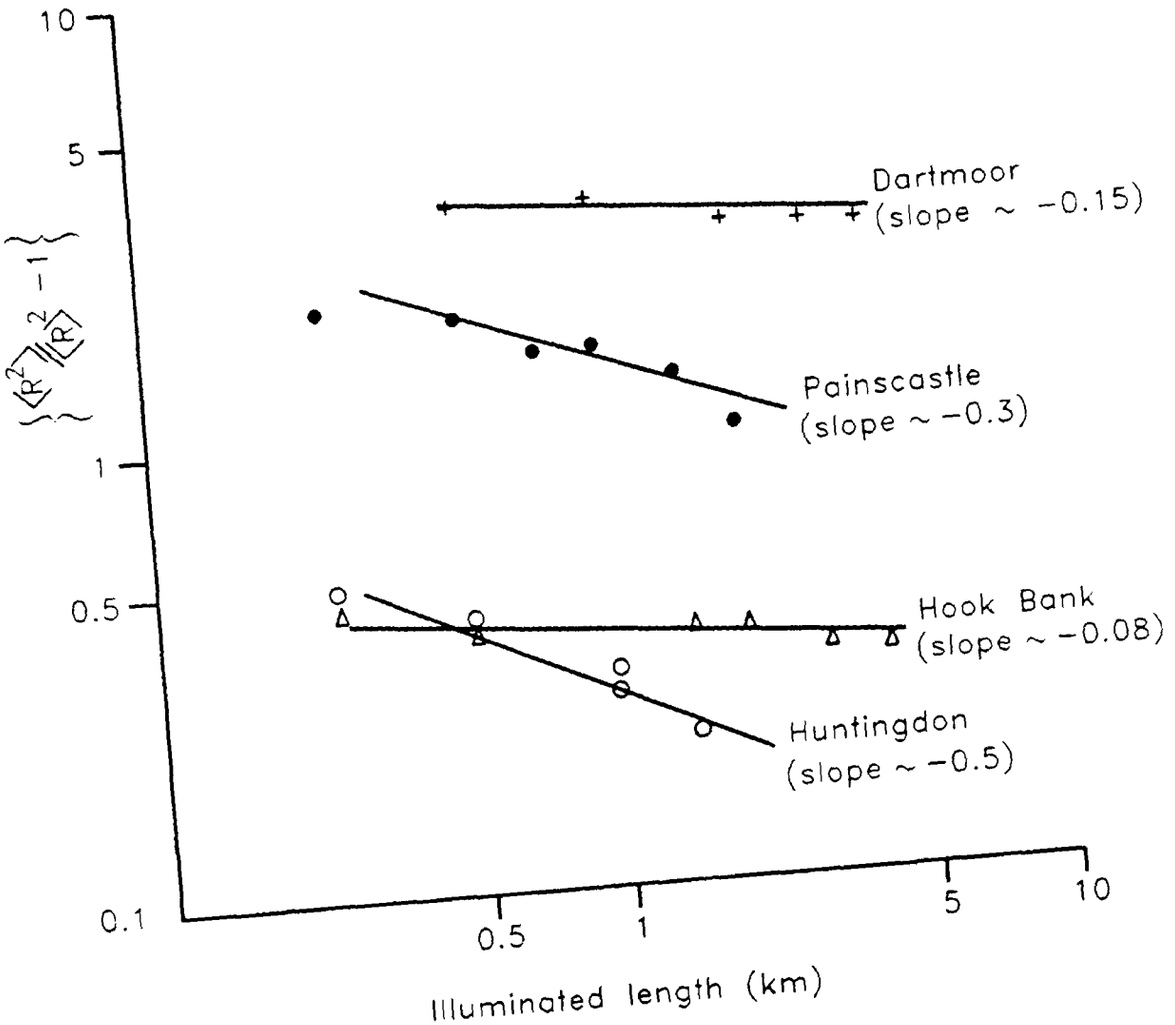
10
5
1
0.5
0.1
0.5
1
5
10
$\langle R^2 \rangle / \langle R \rangle^2 - 1$
Illuminated length (km)
Dartmoor
(slope ~ −0.15)
Painscastle
(slope ~ −0.3)
Hook Bank
(slope ~ −0.08)
Huntingdon
(slope ~ −0.5)

FIGURE 15

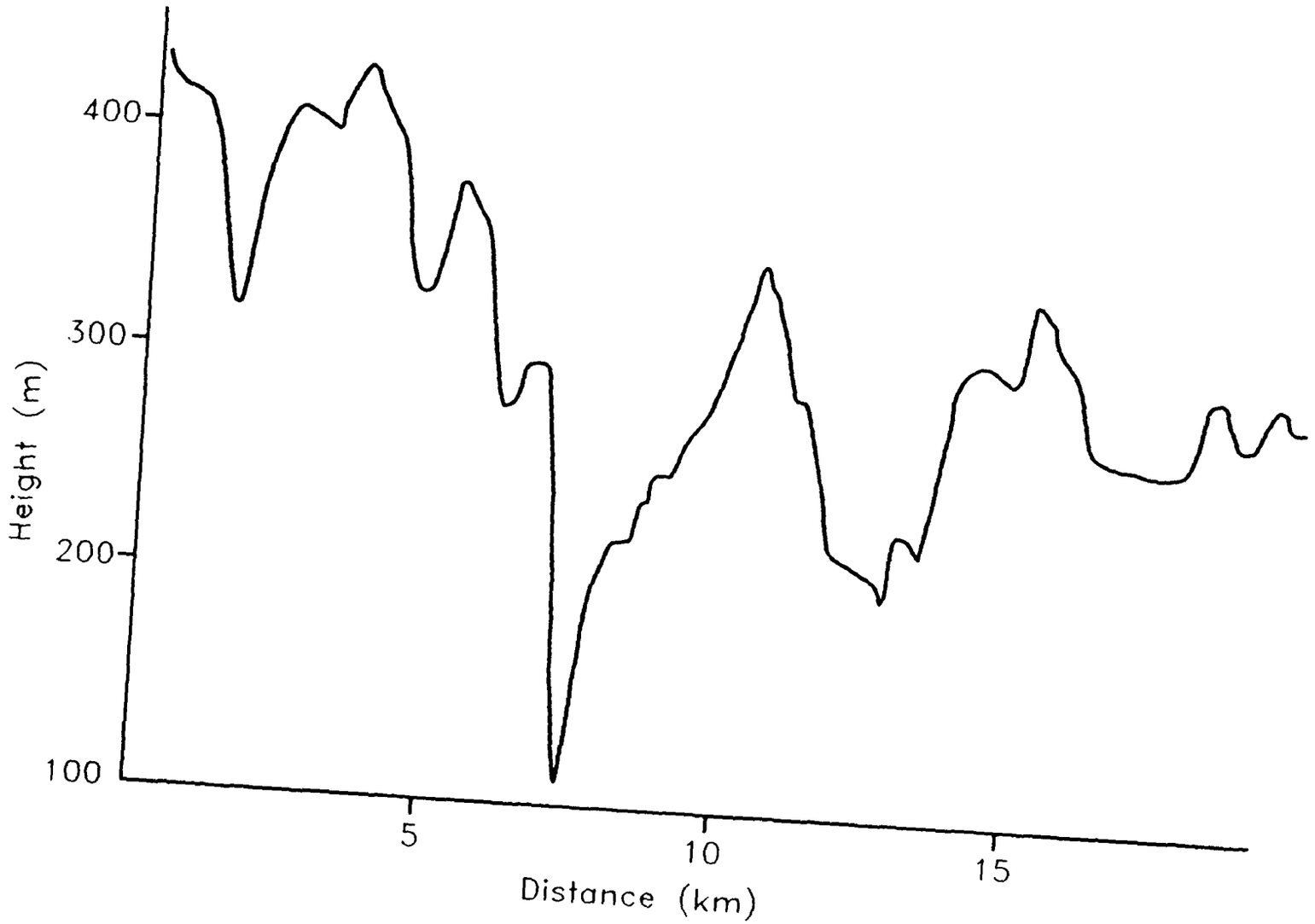

FIGURE 16 (a)

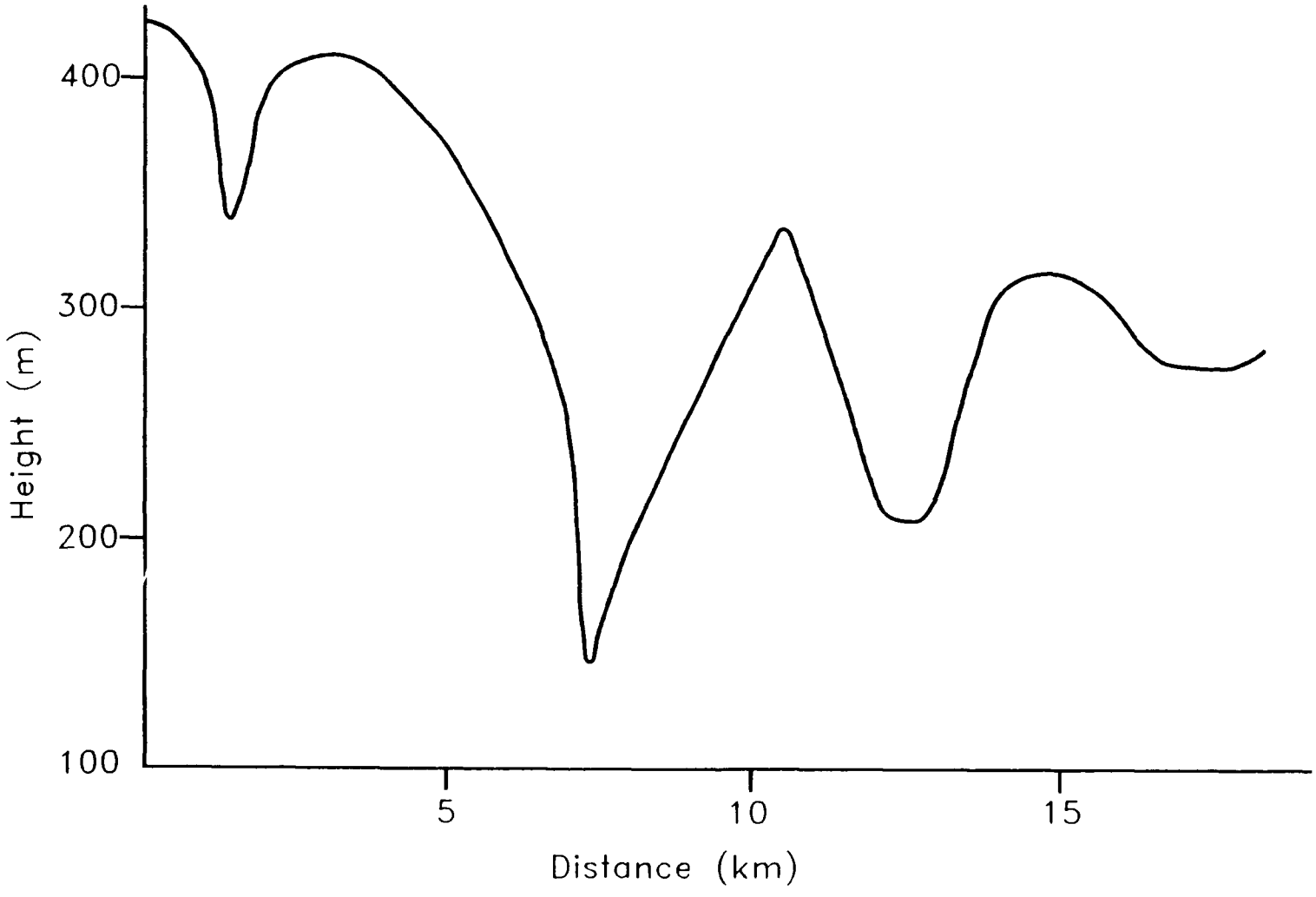

FIGURE 16 (b)

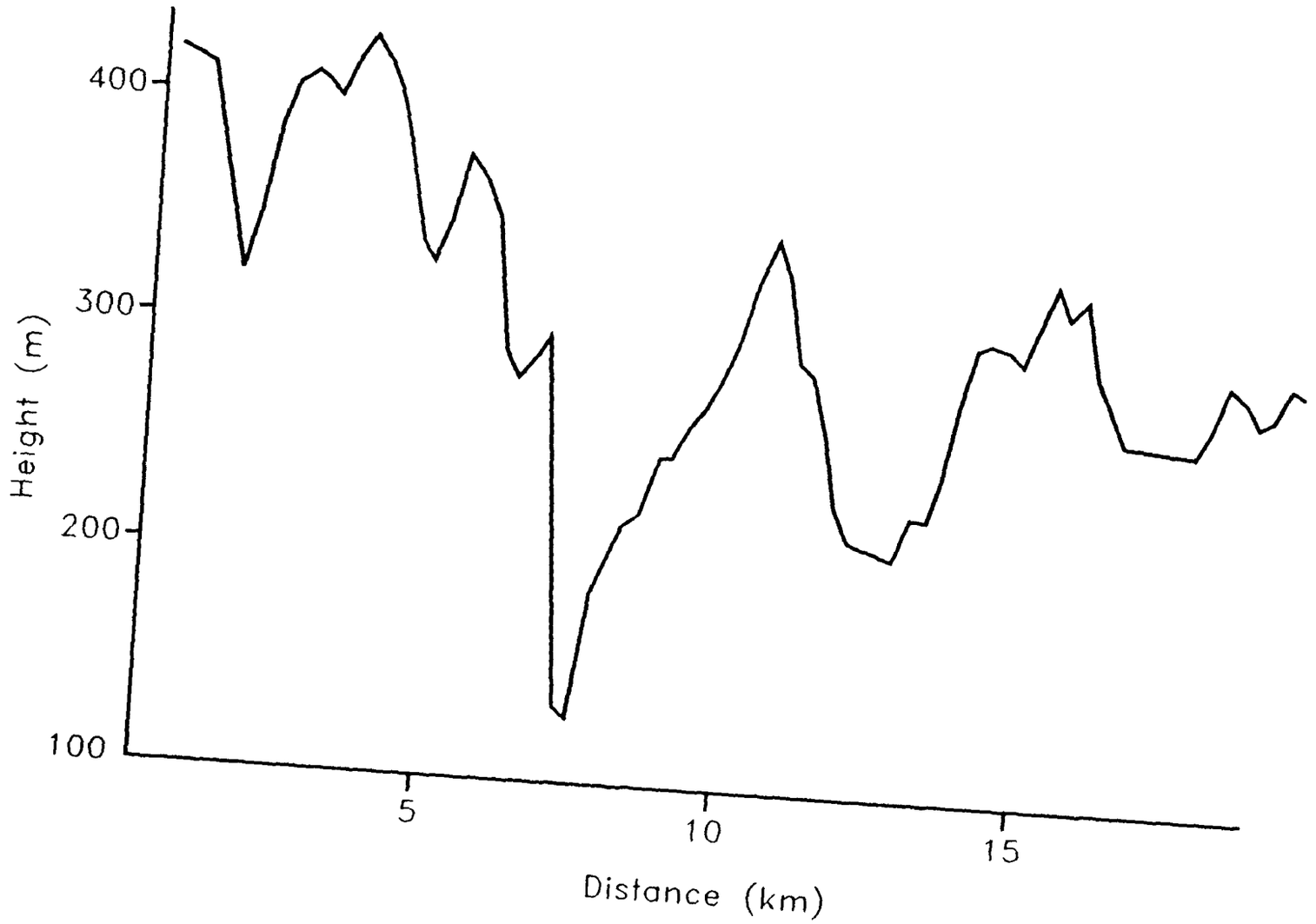

FIGURE 16 (c)

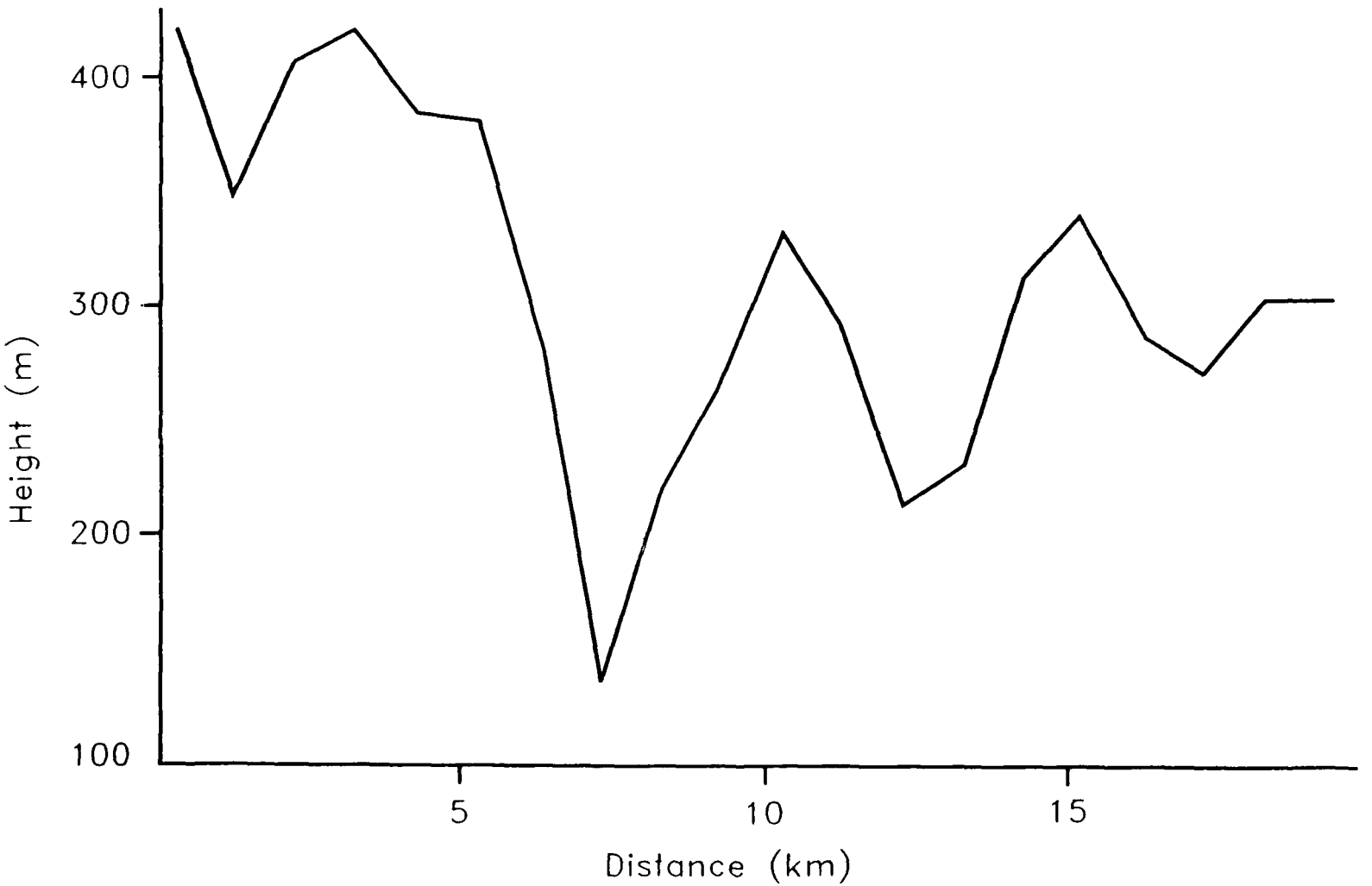

FIGURE 16 (d)

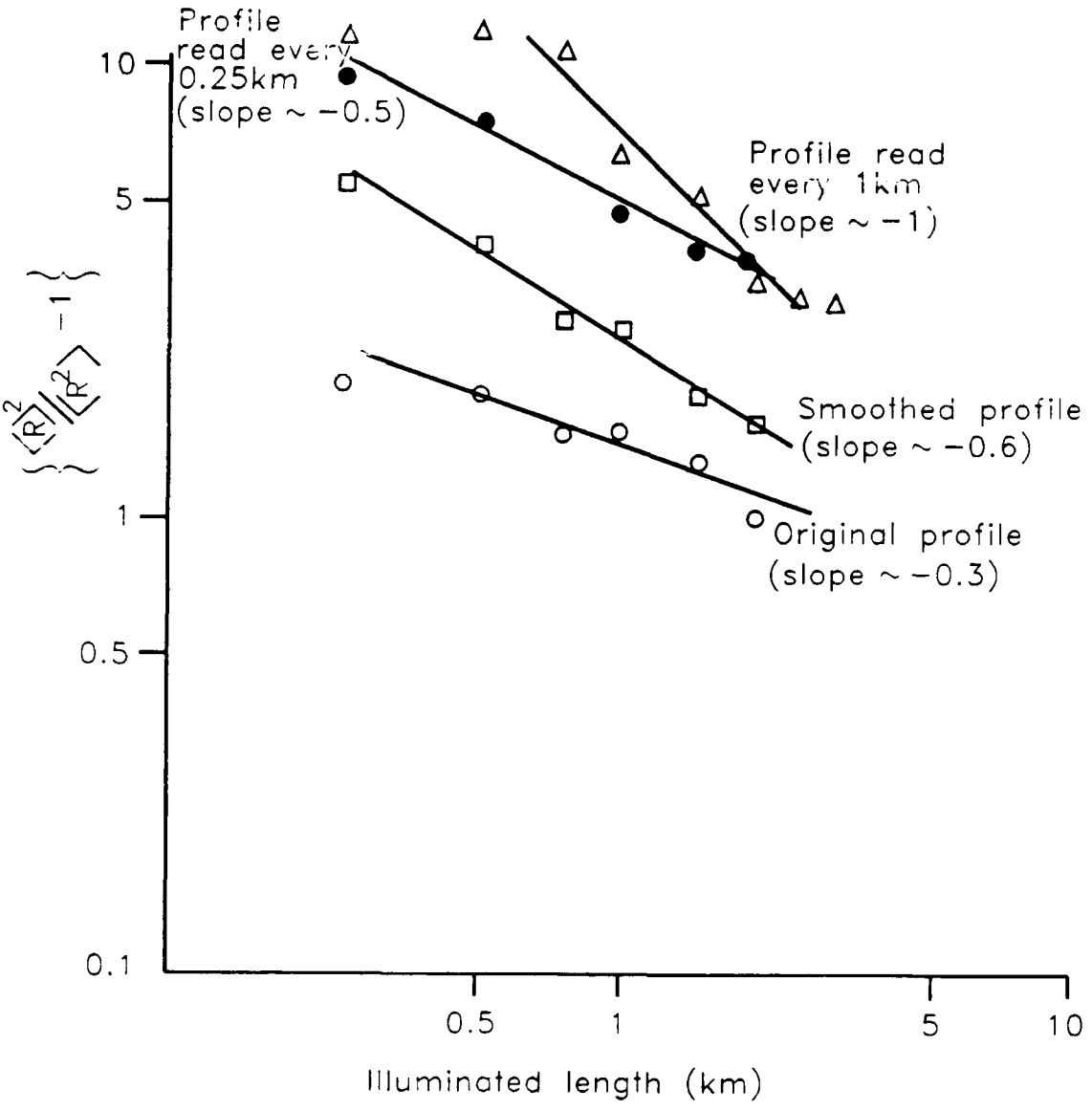
Profile
read every
0.25km
(slope ~ −0.5)
Profile read
every 1km
(slope ~ −1)
Smoothed profile
(slope ~ −0.6)
Original profile
(slope ~ −0.3)
10
5
1
0.5
0.1
0.5
1
5
10
$\{\langle R\rangle^2/\langle R^2\rangle - 1\}$
Illuminated length (km)

FIGURE 17

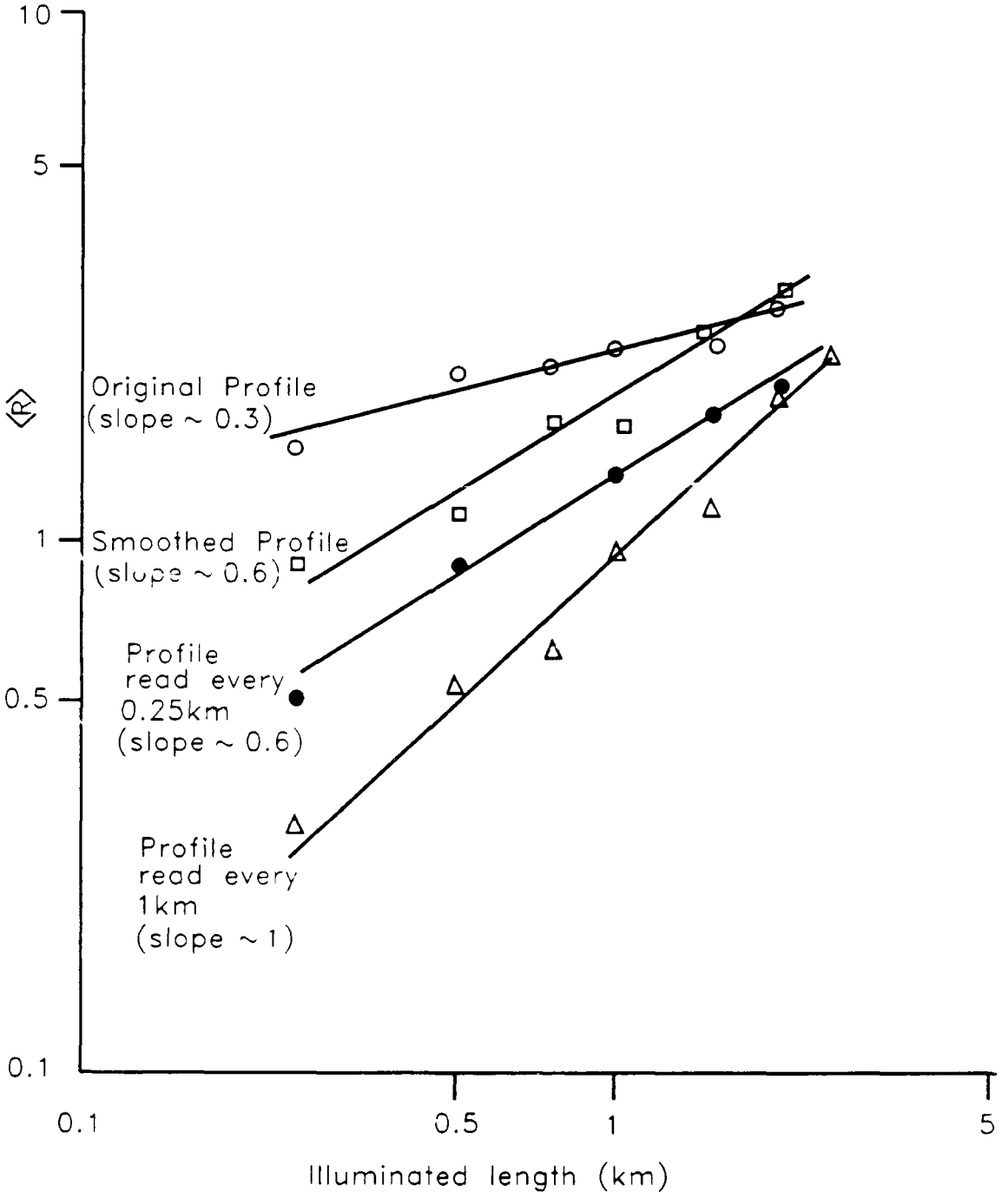
10
5
1
0.5
0.1
⟨R⟩
Original Profile
(slope ~ 0.3)
Smoothed Profile
(slope ~ 0.6)
Profile
read every
0.25km
(slope ~ 0.6)
Profile
read every
1km
(slope ~ 1)
0.1
0.5
1
5
Illuminated length (km)

FIGURE 18

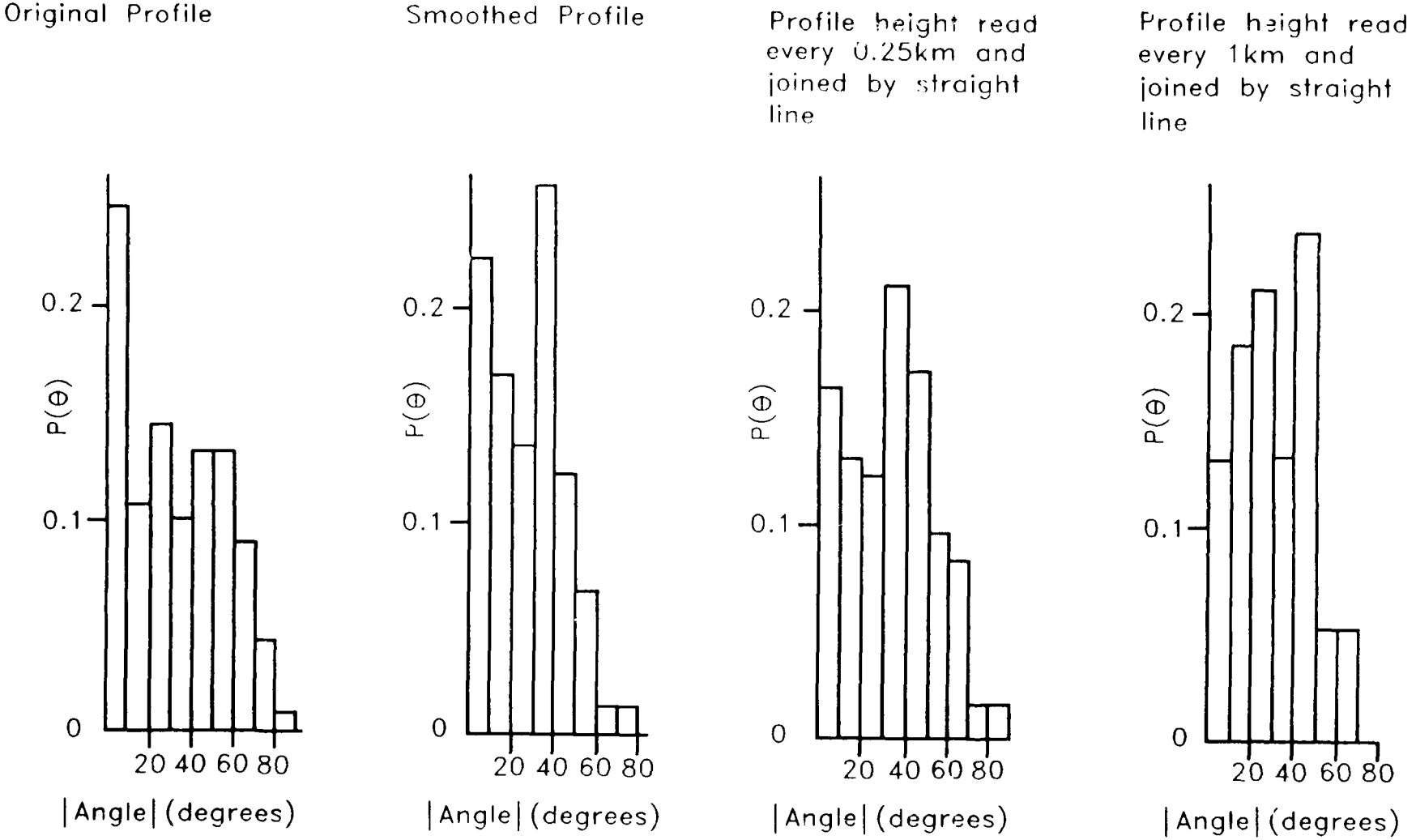
Original Profile
Smoothed Profile
Profile height read every 0.25km and joined by straight line
Profile height read every 1km and joined by straight line
0.2
0.1
0
P(Θ)
20 40 60 80
|Angle| (degrees)

FIGURE 19

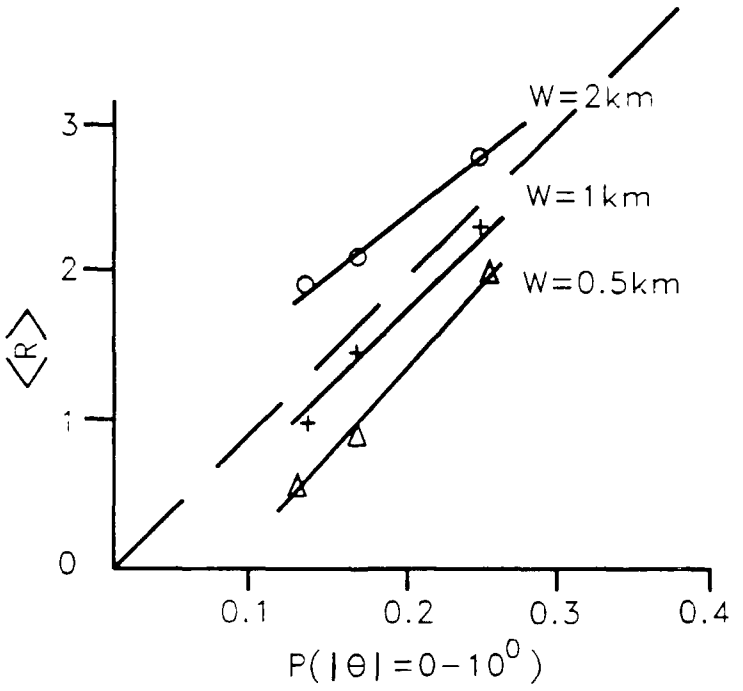

FIGURE 20

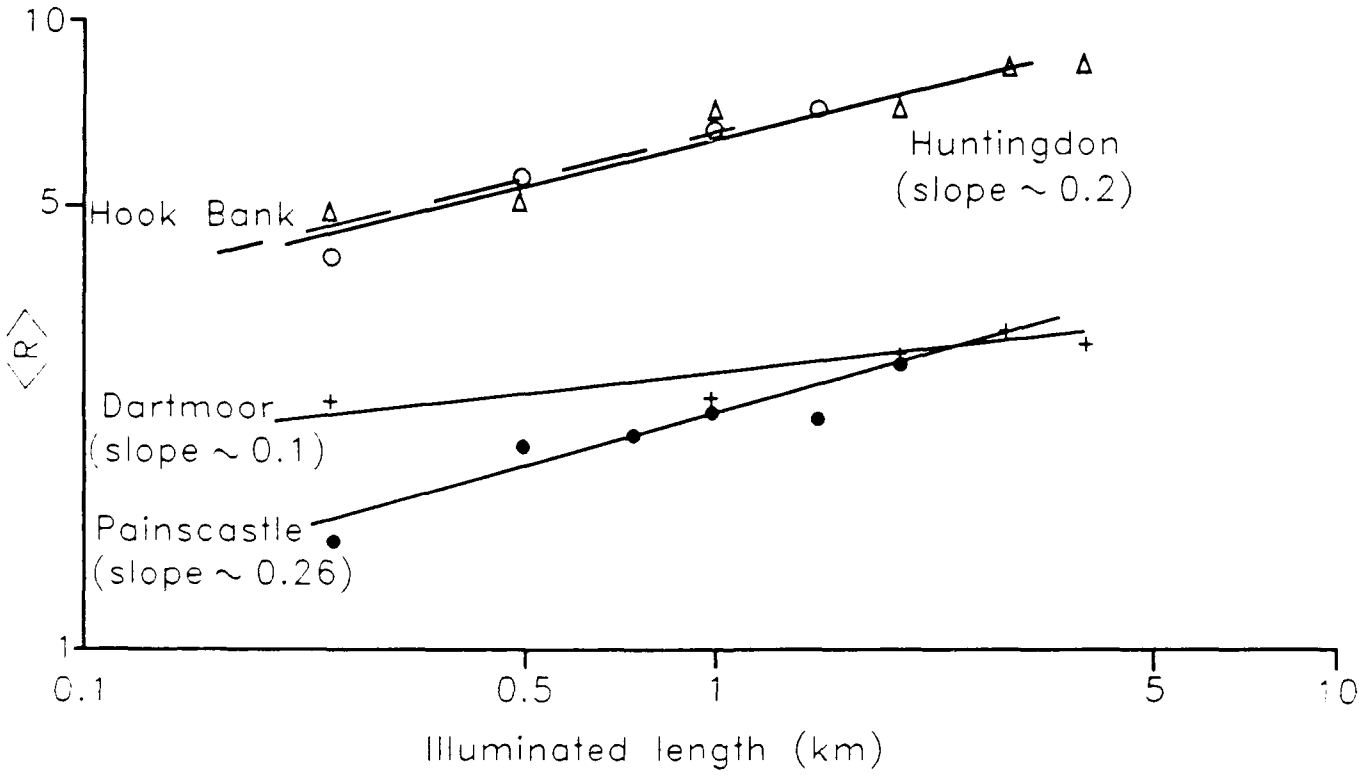
10
5
1
⟨R⟩
Hook Bank
Huntingdon
(slope ~ 0.2)
Dartmoor
(slope ~ 0.1)
Painscastle
(slope ~ 0.26)
0.1
0.5
1
5
10
Illuminated length (km)

FIGURE 21

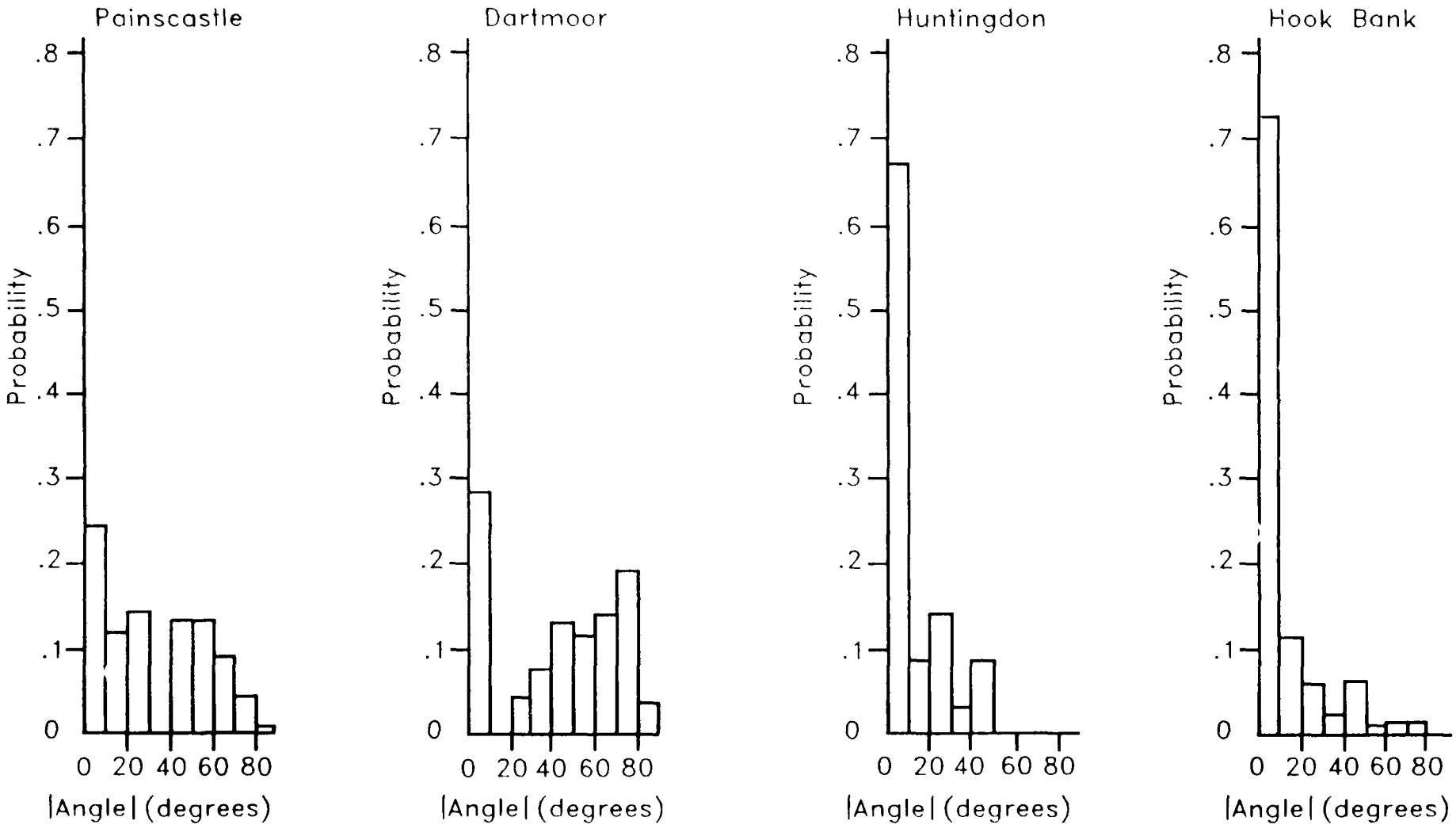
Painscastle
Dartmoor
Huntingdon
Hook Bank
Probability
.8
.7
.6
.5
.4
.3
.2
.1
0
0 20 40 60 80
|Angle| (degrees)

FIGURE 22

DOCUMENT CONTROL SHEET

Overall security classification of sheet ..... UNCLASSIFIED .....

(As far as possible this sheet should contain only unclassified information. If it is necessary to enter classified information, the box concerned must be marked to indicate the classification eg (R) (C) or (S))

1. DRIC Reference (if known)	2. Originator's Reference	3. Agency Reference	4. Report Security Classification
	Memo 4305		U/C

5. Originator's Code (if known)	6. Originator (Corporate Author) Name and Location
7784000	Royal Signals & Radar Establishment St Andrews Road, Great Malvern Worcestershire WR14 3PS
5a. Sponsoring Agency's Code (if known)	6a. Sponsoring Agency (Contract Authority) Name and Location

7. Title Simple Graphical Descriptions of Natural Land Profiles and the Application of Fractal and Sub-Fractal Models to them.

7a. Title in Foreign Language (in the case of translations)

7b. Presented at (for conference papers) Title, place and date of conference

8. Author 1 Surname, initials	9(a) Author 2	9(b) Authors 3,4...	10. Date	pp. ref.
Jordon D L			7.1989	vp

11. Contract Number	12. Period	13. Project	14. Other Reference

15. Distribution statement
UNLIMITED

Descriptors (or keywords)

continue on separate piece of paper

Abstract Terrain profiles from four widely different areas of Britain are obtained from Ordnance Survey maps and shown to be well modelled as either fractal or as a hierarchy of different fractals. The profiles are then smoothed using a crude small-scale smoothing method to allow them to be modelled as sub-fractal surfaces. Rays are drawn from these surfaces to simulate the scattering of incoherent radiation. The resulting ray density statistics are analysed and shown to be approximately Gamma-distributed. Based on the findings suggestions are made regarding possible methods of remotely determining surface texture for metrology purposes. The overall aim of this Memorandum is not mathematical rigour, but rather the use of simple pictorial methods as an aid to gaining a physical insight into rough surface scattering and how such information might be used in describing and measuring surface texture.